SAND2020-4507 R

Hydrogen Fuel Cell Vehicles in Tunnels

Austin M. Glover, Austin R. Baird, Chris B. LaFleur

April 2020

Sandia National Laboratories is a multimission laboratory managed and operated by National Technology and Engineering Solutions of Sandia, LLC, a wholly owned subsidiary of Honeywell International Inc., for the U.S. Department of Energy's National Nuclear Security Administration under contract DE-NA0003525.

ABSTRACT

There are numerous vehicles which utilize alternative fuels, or fuels that differ from typical hydrocarbons such as gasoline and diesel, throughout the world. Alternative vehicles include those running on the combustion of natural gas and propane as well as electrical drive vehicles utilizing batteries or hydrogen as energy storage. Because the number of alternative fuels vehicles is expected to increase significantly, it is important to analyze the hazards and risks involved with these new technologies with respect to the regulations related to specific transport infrastructure, such as bridges and tunnels. This report focuses on hazards presented by hydrogen fuel cell electric vehicles that are different from traditional fuels. There are numerous scientific research and analysis publications on hydrogen hazards in tunnel scenarios; however, compiling the data to make conclusions can be a difficult process for tunnel owners and authorities having jurisdiction over tunnels. This report provides a summary of the available literature characterizing hazards presented by hydrogen fuel cell electric vehicles, including light-duty, medium and heavy-duty, as well as buses. Research characterizing both worst-case and credible scenarios, as well as risk-based analysis, is summarized. Gaps in the research are identified to guide future research efforts to provide a complete analysis of the hazards and recommendations for the safe use of hydrogen fuel cell electric vehicles in tunnels.

ACKNOWLEDGEMENTS

The authors would like to thank the International Partnership for Hydrogen Energy (IPHE) Regulations, Codes, Standards & Safety Working Group (RCSSWG), co-chaired by Pietro Moretto of the European Commission's Joint Research Centre (JRC) and Laura Hill of the U.S. Department of Energy (DOE) Fuel Cell Technologies Office (FCTO), for direction and valuable discussions on this topic. This report was reviewed by members of the workshop on hydrogen vehicles in tunnels and Alice Muna (Sandia), and the authors thank those that provided feedback. Financial support for this effort was provided by the U.S. DOE FCTO.

CONTENTS

LIST OF FIGURES

LIST OF TABLES

ACRONYMS AND DEFINITIONS

Abbreviation	Definition
AIT	auto-ignition temperature
CANA	Central Artery North Area
CFD	computational fluid dynamics
DDT	deflagration-to-detonation transition
DOE	Department of Energy
FCEV	fuel cell electric vehicle
FL	flammability limit
FLACS	FLame ACceleration Simulator
HRR	heat release rate
HSL	Health and Safety Laboratory
IPHE	International Partnership for Hydrogen Energy
ISO	International Organization for Standardization
LEL	lower explosive limit
LFL	lower flammability limit
NFPA	National Fire Protection Association
NIST	National Institute of Standards and Technology
MIE	minimum ignition energy
PRA	probabilistic risk assessment
PRD	pressure relief device
QRA	quantitative risk analysis
RCSSWG	Regulations, Codes, Standards & Safety Working Group
SNL	Sandia National Laboratories
THR	total heat released
TPRD	thermally activated pressure relief device
UEL	upper explosive limit
UFL	upper flammability limit
SNL	Sandia National Laboratories

1. INTRODUCTION

The purpose of this report is to present tunnel owners with concise scientific information about the use of hydrogen fueled electric vehicles in tunnels. The goals of this paper are in line with the goals of the International Partnership for Hydrogen Energy (IPHE) [1] Regulations, Codes, Standards & Safety Working Group (RCSSWG) activities. The RCSSWG provides a forum to identify, discuss, and reach consensus on challenging RCSS issues. Because the RCSSWG is supported under the IPHE, a government partnership, discussion in workshops such as the one which provided the basis for this report are driven by technical content with a focus on solutions which enable harmonization and address barriers to accelerating large-scale deployment of hydrogen and fuel cell technologies. In pursuit of these objectives, the RCSSWG has established a framework for holding meetings in conjunction with established international events in order to leverage the expertise represented there. This paper expands on recent research reviewed at a workshop on hydrogen vehicles in tunnels, held at the Health and Safety Laboratory (HSL), Buxton, UK in September 2018.

At the request of industry as well as state, federal and international government stakeholders, this study was initiated in 2016 and included a range of resources and technical expert feedback, consolidated by Sandia national laboratories. A comprehensive literature review on publicly available tunnel experiments and modeling was compiled which focused on the hazards associated with hydrogen fueled vehicles. After a systematic review of this material, potential research gaps were discussed. This includes a review of the scenarios and failure modes, and the range of consequences associated with the failures. For the scope of this paper, tunnel is defined as a roadway which is enclosed to allow the roadway to pass under a body of water or through rock (i.e. in mountainous terrain). Railway tunnels are not considered in this definition because rail tunnels represent much larger volumes of hydrogen transported as cargo or to fuel the locomotive. Because the volume of fuel is an important consideration, the class of vehicle is noted where applicable to help further understand the consequence of a light-duty, medium-duty, and heavy-duty vehicle incident.

Note that some of the research presented in this document assess theoretical scenarios that are implausible in the real world, such as large stoichiometric mixtures. These situations are included in this paper to recognize the scientific principle, but also point out the improbability of similarly replicating outside a laboratory. However, consequence is only part of the overall risk. The likelihood of these scenarios is extremely low or virtually impossible, which significantly lowers the risk of the theoretical hazards.

1.1. Definitions for Hazard Metrics

The following section defines the various hazard metrics discussed in the literature:

- Flammability Limits

Flammability limits are important for fire and explosion analysis because it defines the volume fraction and conditions range of fuel required to create a flammable environment. Codes, standards, and practices have specific requirements regarding the flammable gas concentration permitted in any given environment. The lower flammability limit (LFL) is the lowest fuel concentration that will allow flame or flash propagation from an ignition source within the mixture. The upper flammability limit (UFL) is the highest fuel concentration that will allow flame or flash propagation from an ignition source within the mixture. Outside of these limits, no flame can occur [2]. Standard units of flammability limits are in volume percent (%) or volume fraction.

- Explosion Limits

Explosion limits refer to the range of pressure and temperature for which an explosive reaction can occur for a fixed composition mixture. The explosion limit is given as a minimum autoignition temperature (AIT) which is a strong function of the fuel type, pressure, and overall fuel concentration [3]. The explosion limits are within the same concentration range as the flammability limits. Standard units of explosion limits are in volume percent (%) or volume fraction.

- Auto-Ignition Temperature

The auto-ignition temperature (AIT) is the lowest recorded temperature in which ignition occurs spontaneously or in the absence of piloted ignition source in a material. This applies to solids, liquids and gases. If the rate at which heat evolves in a gas or vapor is greater than the rate of heat loss to the surrounding area, ignition can result [2] [4]. Standard units for the auto-ignition temperature is degrees Celsius (°C) or degrees Fahrenheit (°F).

- Detonation Limits

Detonation limits is the range at which a detonation can self-sustain. These limits typically have a narrower range within the flammability/explosion limits. This is due to the stronger dependence on confinement, mixture composition, and initial temperature and pressure compared with the flammability/explosion limits [3]. Standard units for detonation limits are in volume percent (%) or volume fraction.

- Laminar Flame Speed

The critical parameter controlling the rate of pressurization is the burning speed. The burning speed is correlated to a fundamental flame propagation rate into the unburned premixed gas. This flame speed generally increases with increasing temperature and decreases with increasing pressure [5]. The laminar flame speed is dependent on the chemical kinetics along with the thermal and mass diffusion [6]. Standard units for the laminar flame speed are meter-per-second (m/s) or feet-per-minute (ft/min).

- Overpressure

Overpressure defines the pressure wave that a flammable mixture generates during combustion. This pressure wave is caused by the energy released from initial deflagration/detonation. The maximum theoretical overpressure (P_{max}) is the pressure that is generated when the gas is combusted in a perfectly adiabatic process in a closed chamber. This is a value generated theoretically or at optimal conditions in a laboratory. P_{max} depends on the composition of gas produced as well as the concentration and other factors such as confinement [7]. Standard units for overpressure can be kilopascals (kPa), pounds-per-square-inch (psi), or bar.

- Equivalence Ratio

The ratio of actual molar fuel/air ratio to the stoichiometric molar fuel/air ratio is the equivalence ratio. If this ratio is below 1, this is a lean mixture with excess air for combustion. If the ratio is above 1, the mixture is fuel rich leading to incomplete combustion. Combustion in stoichiometric conditions leads to complete consumption of oxygen and fuel during a reaction.

- Adiabatic Flame Temperature

Adiabatic flame temperature is the maximum temperature that can result from combustion of reactants. Heat transfer away from the reaction, incomplete combustion, and other dissociations will result in a lower temperature. The maximum adiabatic flame temperature occurs when a mixture is stoichiometric [8]. Standard units for flame temperature are Kelvin (K), degrees Celsius (°C), or degrees Fahrenheit (°F).

- Flash Point

The flash point is the lowest temperature at which a liquid solvent can form a mixture above the surface or within a container that is flammable or ignitable. Lower flash point temperatures indicate that it is easier for the mixture to ignite. There are two types of tests to measure the flash point: closed cup and open cup. These methods test flash point in an open pool type configuration and a closed container configuration [2]. Standard units for the flash point temperature degrees are degrees Celsius (°C) or degrees Fahrenheit (°F).

- Heat of Combustion

Heat of combustion is the amount of heat released when a substance is burned. The heat of combustion can be further defined as the higher and lower heating values. The lower heating value of a fuel is defined by combustion of a fuel at 25°C and returning the resulting mixture of combustion products down to 150°C. This assumes the latent heat of vaporization of water in the reaction products is not recovered. The higher heating value is similar, but the products have returned to a temperature of 25°C, which considers the latent heat of vaporization of water in the combustion products [9]. Standard units for the heat of combustion are Megajoule per Kilogram (MJ/kg), British Thermal Units per-pound-mass (Btu/lb_m), or kilojoule-per-mole (kJ/mol).

- Heat Release Rate

Heat release rate (HRR) is the rate of energy released from a fire. This rate is typically defined by a plotted curve, with time on the horizontal axis and energy released on the vertical axis [10]. The heat release rate curve is used to characterize fires by understanding the peak heat release rate as well as the time the fire lasts. Standard units for the heat release rate are kilowatt (kW) or British Thermal Unit per hour (Btu/hr).

- Heat Flu

In addition to the HRR, the heat release rate flux or heat flux is the total energy flow over time per unit of surface area. Standard units for the heat flux are kilowatt per square meter (kW/m^2) or British Thermal Unit per square foot ($Btu/hr\text{-}ft^2$).

- Total Heat Release

The total area under the heat release rate curve defines the total heat released (THR) [10]. Total heat released is used to characterize the size of a fire. Standard units for the total heat released are megajoule (MJ) or British Thermal Unit (Btu).

1.2. Tenability Criteria

To better understand the consequence and take-away values from the literature review, the following tables illustrate the effects of overpressure, heat flux, and temperature hazards. The severity of

injuries and damage with the increase in these metrics is shown in Table 1 through Table 3. Table 1 lists the human injury criteria due to overpressure from National Fire Protection Association (NFPA) 921: Guide for Fire and Explosion Investigations [11].

Table 1: Human Injury Criteria from Overpressure (from [11])

Overpressure			Effects or Injuries
psi	kPa	bar	
0.60	4.14	0.04	Threshold for injury from flying glass
1.00-2.00	6.90-13.80	0.070-0.140	Threshold for skin laceration from flying glass
2.40-2.80	16.50-19.30	0.170-0.19	Threshold for eardrum rupture/10% probability of eardrum rupture
2.00-3.00	13.80-20.70	0.140-0.21	Threshold for serious wounds from flying glass
3.00	20.70	0.21	Overpressure will hurl a person to the ground
3.40	23.4	0.23	1% eardrum rupture
4.00-5.00	27.60-34.500	0.28-0.35	Serious wounds from flying glass near 50% probability
5.80	40.00	0.40	Threshold for body-wall penetration from flying glass (bare skin)
6.30	43.40	0.43	50% Probability of eardrum rupture
7.00-8.00	48.30-55.20	0.48-0.55	Serious wounds from flying glass near 100% probability
10.00	68.95	0.69	Threshold for lung hemorrhage
14.50	99.97	1.00	Fatality threshold for direct blast effects
16.00	110.30	1.10	50% eardrum rupture
17.50	120.70	1.21	10% probability of fatality from direct blast effects
20.50	141.30	1.41	50% probability of fatality from direct blast effects
25.50	175.80	1.76	90% Probability of fatality from direct blast effects
27.00	186.20	1.86	1% mortality
29	199.9	2.00	99% Probability of fatality from direct blast effects

Table 2 illustrates the levels and exposure durations at which blistering (second-degree burn) injuries occur due to heat flux exposure from NFPA 921: Guide for Fire and Explosion Investigations [11]. Both the heat flux and exposure time help in understanding consequences.

Table 2: Effects from Heat Flux (from [11])

Radiant Heat Flux		Effects or Injuries
kW/m^2	$Btu/hr\text{-}ft^2$	
2.5	793	Common thermal radiation exposure while firefighting. This energy level may cause burn injuries with prolonged exposure.
		Human skin experiences pain with a 33-second exposure and blisters in 79 seconds with second-degree burn injury.
5	1,586	Human skin experiences pain with a 13-second exposure and blisters in 29 seconds with second-degree burn injury.
10	3,172	Human skin experiences pain with a 5-second exposure and blisters in 10 seconds with second-degree burn injury.
15	4,758	Human skin experiences pain with a 3-second exposure and blisters in 6 seconds with second-degree burn injury.
20	6,344	Human skin experiences pain with a 2-second exposure and blisters in 4 seconds with second-degree burn injury.
80	25,377	Heat flux for protective clothing Thermal Protective Performance (TPP) Test.
100	31,720	Steel structure collapse (>30 min exposure) (from [12])

Table 3 illustrates various effects and injuries from temperature exposure from National Institute of Standards and Technology (NIST) [10]. Using this information along with the heat flux is important to help understand the consequences associated with exposure to fire.

Table 3: Human Injury Criteria from Temperature (from [10])

Temperature		Effects or Injuries
Celsius (°C)	Fahrenheit (°F)	
37.0	98.6	Average normal human oral/body temperature
38	101	Typical body core temperature for a working fire fighter
43	109	Human body core temperature that may cause death
44	111	Human skin temperature when pain is felt
48	118	Human skin temperature causing a first-degree burn injury
54	130	Hot water causes a scald burn injury with 30 second exposure
55	121	Human skin temperature with blistering and second degree burn injury
62	140	Temperature when burned human tissue becomes numb
72	162	Human skin temperature at which tissue is instantly destroyed
100	212	Temperature when water boils and produces steam
250	482	Temperature when charring of natural cotton begins
>300	>572	Modern synthetic protective clothing fabrics begin to char
≥400	≥752	Temperature of gases at the beginning of room flashover
≈1000	≈1832	Temperature inside a room undergoing flashover

1.3. Vehicle Classifications

Vehicle classifications are defined by the vehicle's gross vehicle weight rating (GVWR), which is the maximum operating weight of the vehicle. The GVWR includes all vehicle fluids, passengers, and the cargo capability but does not include trailers. Definitions from various administrations such as the U.S. Department of Transportation Federal Highway Administration (FHWA) and U.S. Environmental Protection Agency (EPA) are included along with examples and applications of each vehicle class.

Table 4: Vehicle Weight Classifications (from [13])

Vehicle Class	Examples/ Applications	DOT FHWA	EPA
Light-Duty Vehicle	Sedans, SUVs, Pickups, Utility Van	Class 1: <6,000 lbs.	Heavy-Duty Engine Light Light-Duty Truck: <6,000 lbs.
			Light-Duty Vehicle: <8,500 lbs.
			Light-Duty Trucks: <8,500 lbs.
		Class 2: 6,001 – 10,000 lbs.	Light-Duty Truck 3 and 4 and Heavy Engines Heavy Light-Duty Truck: 6,001 – 8,500 lbs.
			Medium-Duty Vehicle: 8,501 – 10,000 lbs.
Medium-Duty Vehicle	Delivery Truck, Bucket Truck, School Bus	Class 3: 10,001 – 14,000 lbs.	Heavy-Duty Vehicle Heavy-Duty Engine: >8,500 lbs.
			Heavy-Duty Vehicle 3: 10,001 – 14,000 lbs.
		Class 4: 14,001 – 16,000 lbs.	Heavy-Duty Vehicle 4: 14,001 – 16,000 lbs.
		Class 5: 16,001 – 19,500 lbs.	Heavy-Duty Vehicle 5: 16,001 – 19,500 lbs.
		Class 6: 19,501 – 26,000 lbs.	Heavy-Duty Vehicle 6: 19,501 – 26,000 lbs.
Heavy-Duty Vehicle	City Bus, Refuse, Moving Truck, Truck, Fuel Vehicle, Heavy Semi Tractor	Class 7: 26,001 – 33,000 lbs.	Medium Heavy-Duty Engine: 19,501 – 33,000 lbs.
			Heavy-Duty Vehicle 7: 26,001 – 33,000 lbs.
		Class 8: >33,000 lbs.	Heavy Heavy-Duty Engine Urban Bus: >33,000 lbs.
			Heavy-Duty Vehicle 8a: 33,001 – 60,000 lbs.
			Heavy-Duty Vehicle 8b: >60,000 lbs.

From Table 4, there are three distinct vehicle classes: light-duty, medium-duty, and heavy-duty vehicle. These classes are broken down into sub-classes for each specific administration.

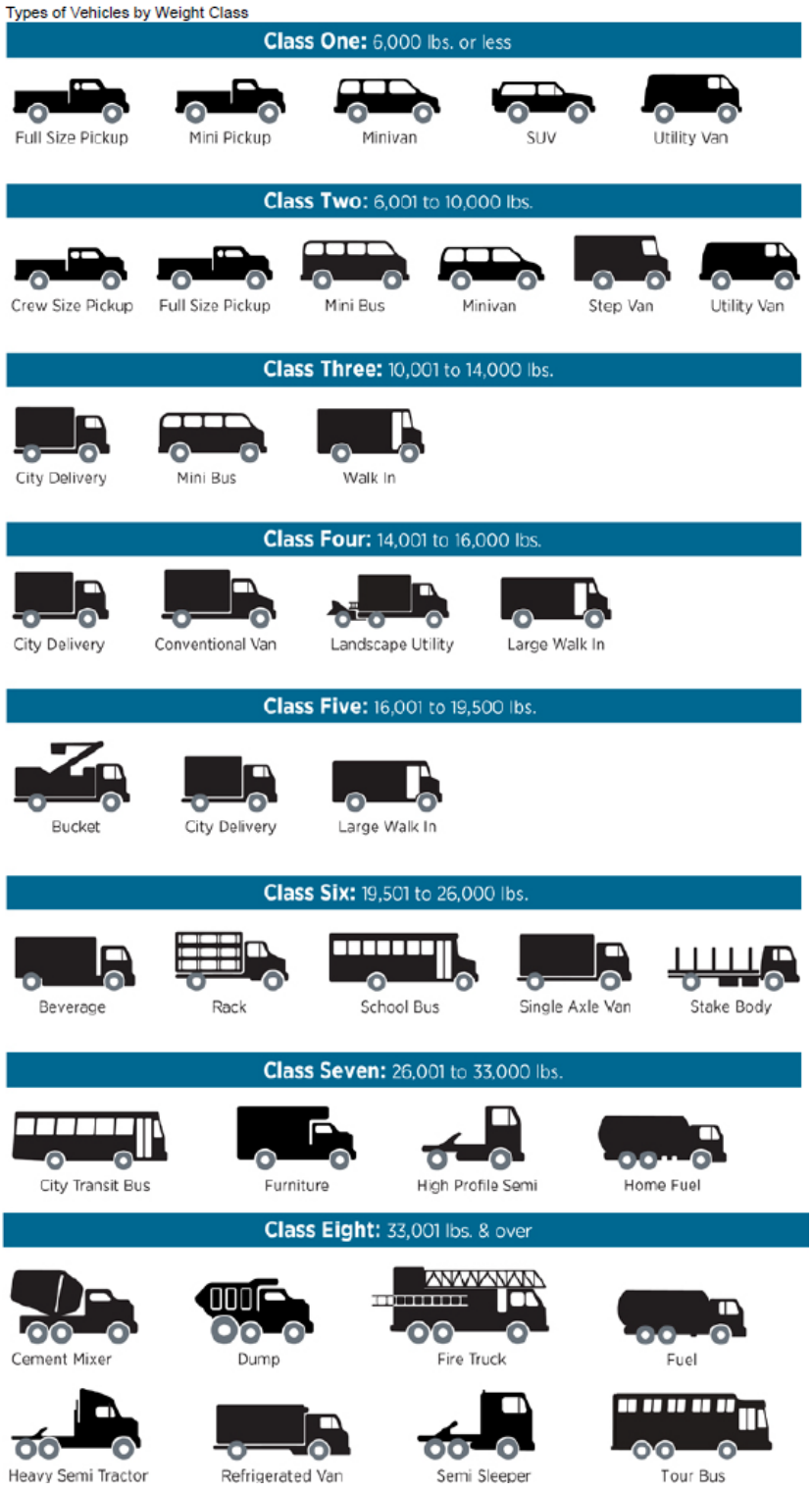

Figure 1: Vehicle Types by Weight Classification (from [14])

Figure 1 above gives further examples of various vehicles and what FHWA weight classification they fall under.

2. HYDROGEN FUEL CELL ELECTRIC VEHICLES

2.1. Overview of Technology

Hydrogen fuel cell electric vehicles (FCEVs) are part of a comprehensive portfolio of technologies and can offer consumers an alternate transportation option to conventional options such as internal combustion engines (ICEs). Fuel cells are more efficient than combustion technologies and FCEVs qualify as zero emission vehicles, emitting no pollution – only water vapor and air through the tailpipe. Additionally, these vehicles offer fast fueling times, and comply with both manufacturer's requirements and consumer expectations for driving range [15]. There are several types of hydrogen FCEVs available to support the diversification of U.S. energy sources in the transportation sector. While there is growing interest in medium and heavy duty FCEVs, production of light-duty hydrogen FCEVs has been ongoing since the Hyundai ix35 fuel cell vehicle rolled off of the assembly line in February of 2013 [16]. An infrastructure of refueling stations has been developed both regionally in the U.S. and in several locations internationally [17]. As of late-2019, there were over 7,800 commercial (sold/leased) fuel cell passenger FCEVs on US roads, mostly in California, with that number projected by industry to exceed 23,000 in 2021 and 47,000 in 2024 [18]. Although these dates and number of deployments may be updated, global industry manufacturers have made a number of plans for commercial expansion, particularly for larger vehicles and trucks, to complement other vehicle platforms such as battery electric vehicles, plug in hybrids, and biofueled ICEs. In addition to FCEVs there are a number of other hydrogen fuel cell applications. For example, there are over ~30,000 fuel cell-powered forklifts operating in commercial warehouses and distribution centers by companies such as Amazon, Coca-Cola, FedEx, Kroger, Walmart, and more as of late-2019 and over 20 million hydrogen fuelings to date [19] [20] [21]. Buses and medium-/heavy-duty vehicles have utilized hydrogen fuel cell technology for public transportation and commodity distribution [22]. The implementation of hydrogen for these larger scale vehicles is expected to increase due to the difficulty in fully decarbonizing these modes of transport. Because of the growing market and diverse applications, a robust safety analysis of hydrogen FCEVs is necessary to ensure public safety.

2.2. Properties of Hydrogen

As an energy carrier, hydrogen fuel can either be a compressed gas or a low-pressure cryogenic liquid. Hydrogen is the lightest gas (~1/14 as dense as air) and at standard temperature and pressure exists in the form of a hydrogen molecule with two atoms: H_2. Liquid hydrogen has a boiling point of -252.88 °C and is much more dense than gaseous hydrogen [23]. Gaseous hydrogen can be stored in high pressure tanks to provide large amounts of energy; however, even more energy can be stored in low pressure cryogenic liquefied form. Hydrogen has an expansion ratio of 1:848, which means that gaseous hydrogen at atmospheric conditions occupies 848 times more volume than liquid hydrogen [24]. Table 5 shows physical and chemical properties of hydrogen [23].

Table 5: Physical and Chemical Properties of Hydrogen (from [23])

Property	Value
Molecular weight	2.0159
Gas Density	0.08988 g/L @ 0°C, 1 atm
Relative Vapor Density	0.07
Liquid Density	70.8 g/L @ -253°C
Melting Point	-259.35°C
Boiling Point	-252.88°C
Auto-ignition Temperature	500°C
Flammability Limits	4-75% (vol % in air)

2.3. Associated Hazards

The primary safety hazard associated with hydrogen is that it is flammable. Hydrogen properties require that the fuel delivery system be designed to mitigate all relevant safety hazards. Table 6 shows relevant flammability properties of hydrogen as compared to other common fuel sources.

Table 6: Flammability Properties of Hydrogen and Other Fuels

Property		Hydrogen	Methane	Propane	Gasoline Vapor
Flammability Concentration in Air (vol%) [25]	LFL	4.0%	5.0%	2.1%	1.2%
	UFL	75.0%	15.0%	9.5%	7.1%
Most Easily Ignited Mixture in Air (vol%)		29% [26]	8.5% [27]	4% [28]	2% [29]
Adiabatic Flame Temperature [30]		2483 K	2236 K	2250 K	2289 K
Buoyancy (ratio to air)		0.07	0.54	1.52	4
MIE [31] [32]		0.011-0.017 mJ	0.28-0.30 mJ	0.25-0.26 mJ	0.8 mJ
Autoignition Temperature [33]		500 °C	580 °C	455 °C	246 – 280 °C

Although hydrogen's lower flammability limit is comparable to the other fuels, it has a much higher upper flammability limit. Also, its minimum ignition energy (MIE) is an order of magnitude lower than the other fuel types. This introduces the possibility of ignition even from weak electrostatic discharged. Sources such as NFPA 77 [34] give discharge ranges showing that even a corona type discharge at the end of a wire or other point could lead to enough energy to exceed the MIE for hydrogen. Figure 2 illustrates the MIE of different fuels as a function of concentration in air by volume. As shown in the figure, between approximately 10% and 60% volumetric concentration, hydrogen has a lower ignition energy than methane and gasoline over a much wider range of

concentration. However, for hazard evaluation the MIE of lean mixtures is more relevant, and hydrogen does not differ from other fuels. At the LFL concentrations for each of the fuels, the ignition energies are much more similar between fuels.

However, it should be noted that these characteristics have led to robust system safety requirements to reduce the likelihood of hydrogen release after an accident.

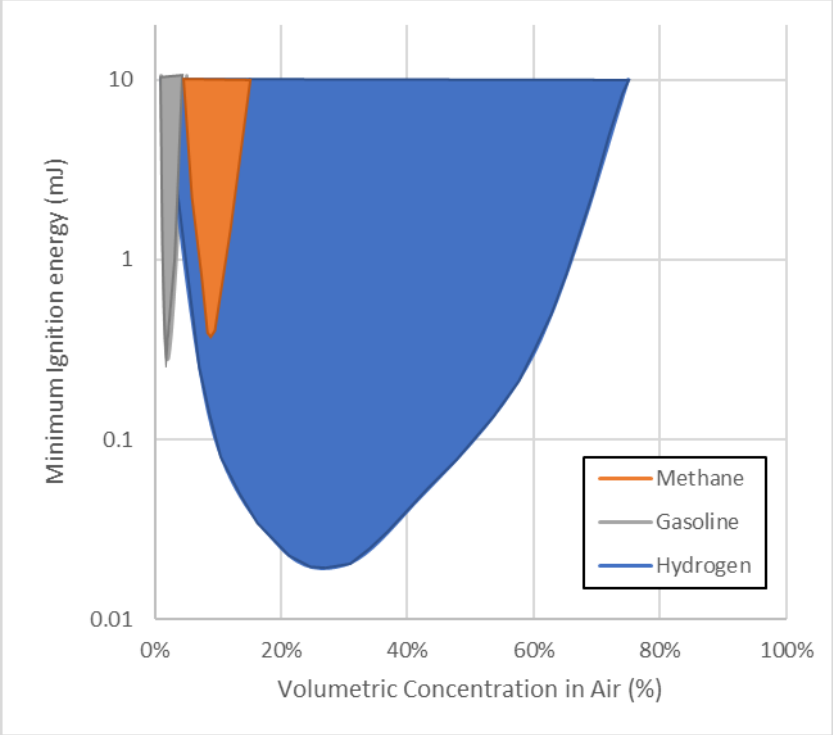

Figure 2: Minimum Ignition Energy for Different Fuels vs. Concentration (from [35])

To mitigate the ignition hazards of hydrogen, sensors are placed in indoor and enclosed locations where hydrogen has the potential to be trapped and accumulate flammable concentrations. These sensors can be programmed to alert when the hydrogen reaches some fraction of the LFL. Because hydrogen is lighter than air, sensors should be placed above potential release points but below ceiling height to avoid elevated temperatures. Consideration should be given to understand the effect of ventilation systems and how air flow might be altered [36]. Most of the hydrogen fuel system will be at a pressure that will result in momentum driven jets of hydrogen. In outdoor locations, hydrogen releases rise away from ignition sources because it is more buoyant than air. This means that hydrogen leaks can dissipate readily, potentially avoiding a concentrated, explosive atmosphere.

2.4. Pertinent Regulations and Safety Standards

Hydrogen FCEVs have robust safety standards and regulations regarding the fuel storage system, the vehicle itself, and the roadway structures on which they operate. The Global Technical Regulation No. 13 (GTR #13) establishes vehicle requirements for hydrogen FCEVs that can attain equivalent levels of safety as those for conventional gasoline powered vehicles. GTR#13 is intended to be applied globally. However, it is up to specific regulatory bodies in each country to adopt the GTR. Because of the large number of countries implementing hydrogen vehicles and developing their jurisdiction-specific requirements, especially for tunnels, this report does not attempt to catalogue these requirements and regulations. However, during the IPHE RCSS Working group meeting in September 2018, many of those present shared the regulations regarding tunnels and enclosed spaces.

Hydrogen vehicle fuel is contained in a composite overwrapped pressure vessel and stored in the gaseous state. The pressure vessel includes a thermal pressure relief device which, in the event of a fire, releases the hydrogen to prevent the vessel from over-pressurizing. Current storage systems have pressures of up to 10 ksi (70MPa). GTR #13 provides requirements for the integrity of compressed and liquid hydrogen motor vehicle fuel systems, including pressure cycling tests, a burst test, a permeation test, and a bonfire test. The pressure cycling test evaluates a container's durability to withstand, without burst, 22,000 cycles of pressurization and depressurization. The burst test evaluates a container's initial strength and resistance to degradation over time. The bonfire test evaluates the ability of the container's thermal pressure relief device to open in a fire scenario (localized and engulfing) [37].

For Crash testing, GTR #13 specifies that participating countries will use existing national crash tests but develop and agree on maximum allowable levels of hydrogen leakage. In the U.S., these national crash tests are found in the Federal Motor Vehicle Safety Standards (FMVSS) which includes specified tests for barrier impacts, rear collisions, and side impact crashes. In a later phase of the requirement, the international crash test requirements are planned to be unified for FCEVs [38].

3. RESEARCH SUMMARY IN TUNNELS

There has been substantial work in evaluating the effects of a failure of a hydrogen tank on an FCEV in a tunnel. This section documents the results of these evaluations.

3.1. Experiments

Several experiments have evaluated the consequences of a hydrogen FCEV failure in a tunnel. A series of experiments were performed to determine what would happen if hydrogen is released from the onboard pressure vessel. It was determined that spontaneous ignition is the most likely consequence (see Section 3.1.1). Qualitatively, this is the least severe and most likely consequence to a hydrogen release in a tunnel. However, there were also several experiments performed to evaluate more severe consequences. Multiple experiments were conducted to evaluate deflagration of hydrogen within a tunnel. These experiments investigated the consequences to delayed ignition of the released hydrogen, considered a worst-case scenario because if ignition does not occur immediately, a large volume of flammable gas could build up and impart more energy into the confined space of a tunnel once it does ignite. An immediate ignition scenario involves less accumulation of hydrogen involved in the ignition event. The concentration of hydrogen and presence of ventilation had a significant effect on the measured pressure pulses (see Section 3.1.2). A variety of quiescent and steady-state hydrogen ignition experiments were performed to evaluate the effect of congestion, hydrogen release rates, along with ventilation rates on overpressure. In general, congestion increased overpressure; however, low hydrogen leakage rates and increased ventilation air velocity resulted in lower overpressure (see Section 3.1.4). Also, deflagration was examined in stratified hydrogen layers to evaluate the potential of self-sustained detonation in flat layer hydrogen-air mixtures. The results indicated that a DDT was possible, however, a minimum layer thickness and sufficient congestion was required (see Section 3.1.5). A series of fire experiments and simulations of a car carrier in a tunnel loaded with hydrogen FCEVs simulated the HRR and showed similar results when compared to the experimental results (see Section 3.1.6). Also, experiments have been performed to validate the results of CFD models (see Section 3.1.3).

3.1.1. Spontaneous Ignition of Pressurized Releases of Hydrogen into Air

A series of experiments were performed to show that the spontaneous ignition of released hydrogen is caused by transient shock formation and mixing associated with rupture of a burst disk between compressed hydrogen and air [39]. Several different variables were evaluated through these experiments, including rupture pressure and internal geometry downstream of the burst disk. The rupture pressure of the burst disk was evaluated with both commercial and in-house manufactured disks with different rupture pressures. The majority of experimentation was performed outdoors, with ambient conditions (between 280K and 305K, with between 60-90% relative humidity). Figure 3 shows a schematic of the experimental configuration [39].

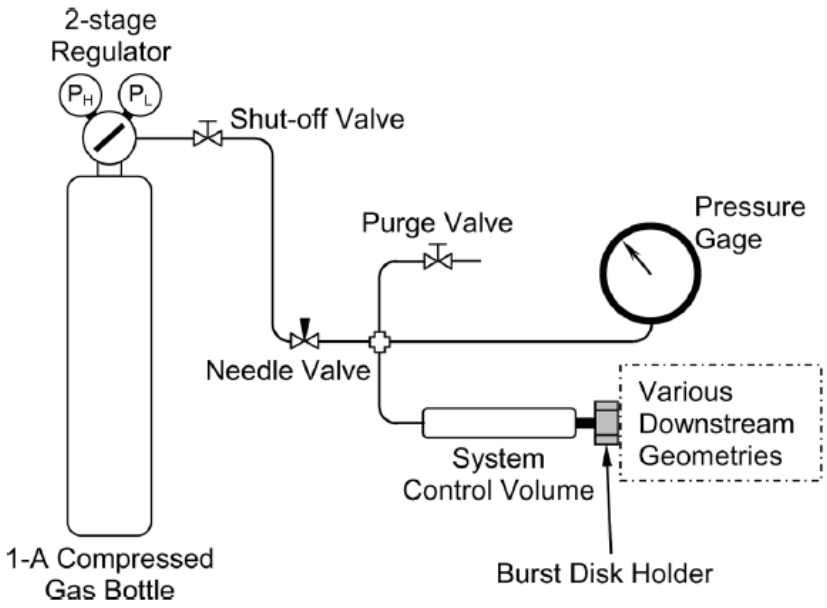

Figure 3: Schematic of Experimental Configuration (from [39])

Over 200 experiments were conducted with hydrogen failure pressures between 11.2 atm and 113.25 atm, with various upstream and downstream geometries. These experiments demonstrated that spontaneous ignition of compressed flammable hydrogen repeatably occurs at the range of pressures seen in FCEV applications, given that sufficient mixing occurs as well. The short mixing time scales are provided by the pressure boundary failure geometry, multi-dimensional shock-boundary, the shock-shock interactions, and the molecular diffusion. Continued combustion can occur because the turbulent free jet hydrogen flames can be stabilized at sufficiently high jet velocities. The reflected shock and shock-shock interactions determine the minimum compressed hydrogen pressure at which spontaneous ignition occurs. Due to the repeatability of the ignition and the characteristic time scale, it was determined that alternative ignition sources, such as electrostatic discharge, did not contribute to these experimental results [39].

3.1.2. Large-scale Hydrogen Deflagrations and Detonations

A scaled down tunnel was used to perform spark-initiated deflagration tests using homogeneous hydrogen mixtures by Groethe et al. [40]. A 1/5-scale tunnel was used to perform multiple experiments with varying released quantities of hydrogen with and without ventilation. This was done to simulate the release from a fuel cell vehicle or storage cylinder on a hydrogen transport. Additionally, selected tunnel tests contained obstacles representing traffic to investigate turbulent enhancement. The cross-area blockage ratio was 0.03. Figure 4 and Figure 5 show the tunnel facility and model vehicles in the tunnel, respectively. Hydrogen was contained in a 37 m^3 volume at the center of the tunnel by HDPE plastic film barriers in homogeneous mixtures ranging from 9.5% (0.32 kg) to 30% (1 kg) hydrogen mixed with air in that volume. Prior to the spark ignition, the plastic barriers were cut. Additional experiments evaluated different release rates of hydrogen both with and without forced ventilation [40].

Figure 4: SRI Corral Hollow Experiment Site Tunnel Facility (from [40])

Figure 5: Model of Vehicles in Tunnel (from [40])

The results of the experiments showed that the 9.5% homogeneous hydrogen mixture produced pressure pulses that were too small for sensors to detect. When the hydrogen content in the mixture was increased to 20% and 30%, the pressure pulses measured 35 kPa and 150 kPa, respectively. It was shown that the presence of the vehicles had an insignificant effect on the deflagration as shown by the pressure pulse, but that ventilation during a release reduces the hazard dramatically. Also, release of hydrogen through a source like the vehicle fuel tank safety release valve produced very lean hydrogen concentrations which created very small pressure pulses [40]. Figure 6 below shows the pressure impulse and overpressure associated with the 30% hydrogen experiment:

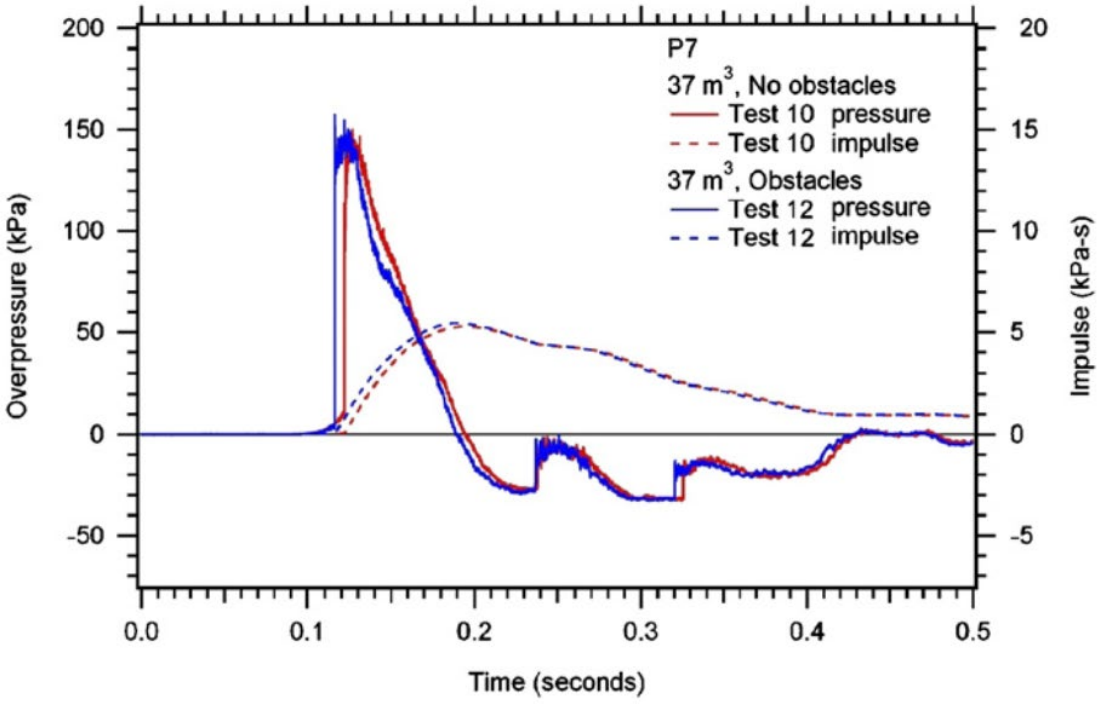

Figure 6: 1/5th Scaled Tunnel Impulse and Overpressure (from [40])

As the Groethe et al. points out, larger vehicles should be studied in this scaled experiment to understand the results. The scaling on how the overpressure changes with the size of tunnel and vehicle would need to be further investigated. As noted by Groethe, the tunnel has a larger aspect ratio than a normal tunnel, which might affect how these results scale up. This directly correlates to the L/D ratio or the length of the tunnel compared to the effective hydraulic diameter. Additionally, to compare with the other literature, the location of the overpressure measurements would need to be well known. Also, known scaling laws such as Hopkinson Blast Scaling and Sachs Blast Scaling could be used to help understand the total explosive energy. Sachs scaling law states that pressure, time, impulse, and other parameters can be expressed as functions of this scaled distance but assumes that air behaves as a perfect gas and assumes gravity and viscosity are negligible [41]. Additionally, how effects of confinement that could lead to turbulent flame speeds might not carry over at full scale. Further understanding these scaling laws would allow for better comparisons between experiments. Studies such as the one by Tamanini [42] provide additional insight on various scaling methods for sizing deflagration vents which helps understand important scaling factors.

3.1.3. Releases from Hydrogen Fuel-cell Vehicles in Tunnels

In order to validate the dispersion/deflagration modeling described in Section 3.2.4, a set of experiments were performed at the SRI Corral Hollow Experiment Site (see Figure 4) by Houf et al. [43]. A set of scaled tunnel tests were performed to approximate the full-scale dimensions of the tunnel from the modeling effort. The hydrogen mass, release rate, initial tank pressure, and TPRD release diameter were scaled to approximate the modeling parameters. Figure 7 shows a comparison of the peak overpressures from the experiments with the results from the model simulations. The peak overpressure from the experiments is in good agreement with the modeling results [43].

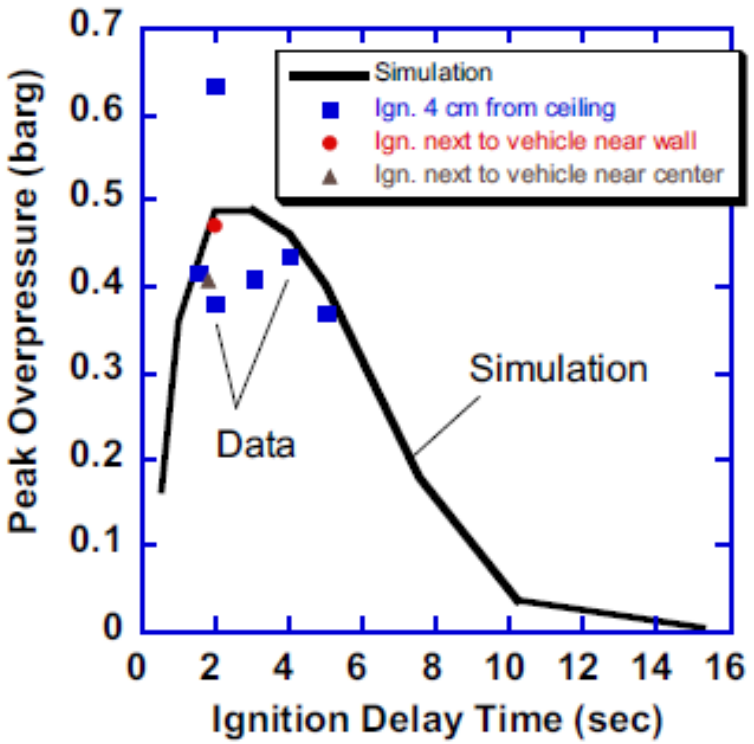

Figure 7: Comparison of Experimental and Modeling Results (from [43])

Figure 8 shows a comparison of the hydrogen concentration at discrete locations within the tunnel as a function of time. As shown, the predicted and measured values are generally in good agreement [43]. While the simulation does approximate the overpressure there are some points in the data that might be considered outliers.

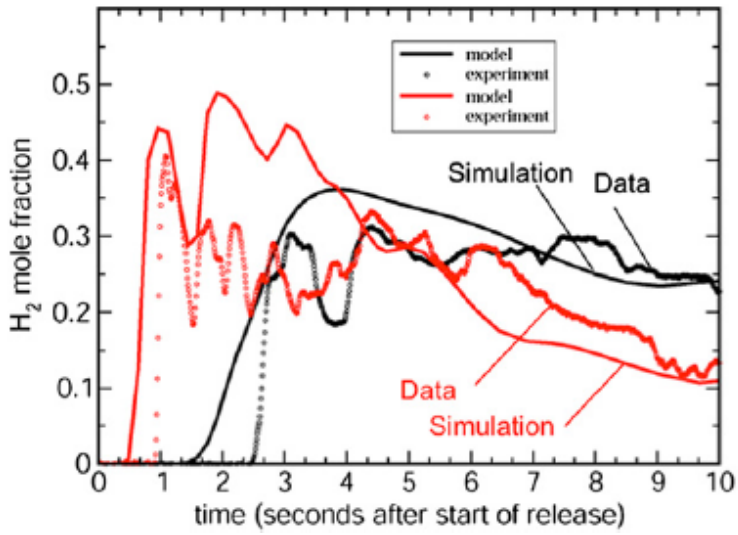

Figure 8: Comparison of Time-dependent Hydrogen Concentration Values (from [43])

3.1.4. HyTunnel Project to Investigate Hydrogen Vehicles in Road Tunnels

A set of experiments were performed by Kumar et al. [44] at the Health and Safety Laboratory to evaluate the influence of congestion and ventilation flow rates on the over-pressure produced from ignition of hydrogen stoichiometric clouds. Quiescent experiments were performed in a sealed enclosure with a stoichiometric hydrogen/air mixture and different congestion volumes/configurations. The congestion configurations consisted of different arrangement of pipes with variable spacing and orientation. Arrangement A is the tight configuration, consisting of four rows of pipes with a spacing of three diameters between pipes, with adjacent rows oriented at right angles and the pipes staggered between every other row. Arrangement B is the loose configuration, consisting of 3 rows of pipes with a spacing of five pipe diameters between pipes, and the same orientation of pipes as Arrangement A. Figure 9 shows the configuration of the ignition experiments. The enclosure (left) shows two modules; however, for the ignition experiments, a total of six modules were combined to give the enclosure a total length of 14.9 m and a volume of 93.1 m^3. The arrangement of the tight congestion setup is also shown (right) [44]. A single obstacle setup is used in each experiment which is shown in Figure 9.

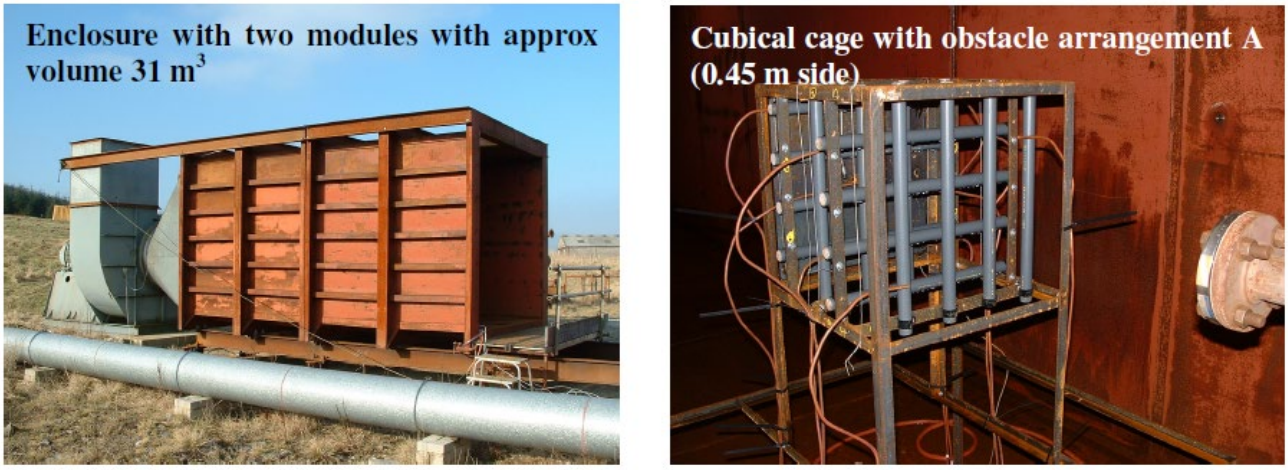

Figure 9: Configuration in Ignition Experiments (from [44])

Table 7 and Figure 8 show the results of the quiescent ignition experiments. A non-uniform pressure field resulted from these hydrogen ignition experiments. An increase in the volume of hydrogen/air mixture increased the maximum explosion overpressure. However, as shown in the table below, an initial increase in the congestion level increased the maximum explosion overpressures (from none to congestion configuration B). Further increase in congestion (from configuration B to configuration A) resulted in a reduction in overpressure [44].

Also, a set of steady-state experiments were performed with various hydrogen leak rates and ventilation flow rates (while also evaluating congestion arrangements A and B). Ventilation in the enclosure was produced through a variable speed fan producing suction through an end plate with 324 circular holes to create a homogeneous flow. Table 7 shows the results of the steady state ignition experiments. As shown, the maximum explosion overpressures increased with increasing hydrogen release rate and decreasing ventilation air velocity. At the lowest leakage rates, the highest explosion overpressures were seen for the more congested configurations. However, at the highest hydrogen leakage rates, the highest explosion overpressures were seen for the less congested configuration (except at the lowest ventilation rate) [44].

Table 7: Results of Steady State Ignition Experiments (from [44])

Hydrogen Release Rate	Air Velocity	Congestion Configuration	Overpressure from Transducer (mbar)		
			Enclosure Left-Hand Wall	Congested Volume Cage Wall Center	Enclosure Right-Hand Wall
1.5 g/s	1 m/s	A	28.2	124.2	63.5
		B	16.2	63.4	19.6
	2 m/s	A	13.6	66.6	12.6
		B	8.8	20.6	7.5
	4 m/s	A	12.1	39.5	10.5
		B	6	13.1	5
2.0 g/s	1 m/s	A	32.4	123.3	55.4
		B	27.5	106	46.6
	2 m/s	A	23.2	117.7	39.6
		B	25.7	66.3	46.6
	4 m/s	A	14.1	53.6	14.7
		B	39.4	25.4	28.9
4.0 g/s	1 m/s	A	48.9	255.8	71.2
		B	48.5	136.9	91.7
	2 m/s	A	37.3	222.5	66
		B	48.1	196.4	85.8
	4 m/s	A	26	160.4	39.2
		B	28.9	126.2	51.2

Table 8: Results of Quiescent Ignition Experiments (from [44])

Congested Volume	Congestion Configuration	Overpressure from Transducer (mbar)	
		Enclosure Left-Hand Wall	Enclosure Right-Hand Wall
0.098% of total enclosure volume	None	28.2	24.7
	B	37.2	42
	A	27.4	24.2
0.55% of total enclosure volume	None	Over-range	85
	B	Over-range	114.6

3.1.5. Deflagration and Detonation of Hydrogen under a Tunnel Ceiling

A set of experiments were performed at Research Centre Karlsruhe in Germany by Friedrich et al. [45] that examined deflagration in stratified hydrogen layers to evaluate the potential of self-sustained detonation in flat mixture layers. Figure 10 shows the main experimental set up used in these evaluations. The chamber had dimensions of 5.7 m x 1.6 m x 0.6 m with layering heights of 0.15 m, 0.3 m, and 0.6 m. The hydrogen concentrations used in these experiments ranged between 15% and 25% (by volume in air). Also, variation in obstacles and hydrogen layer thickness were evaluated [45].

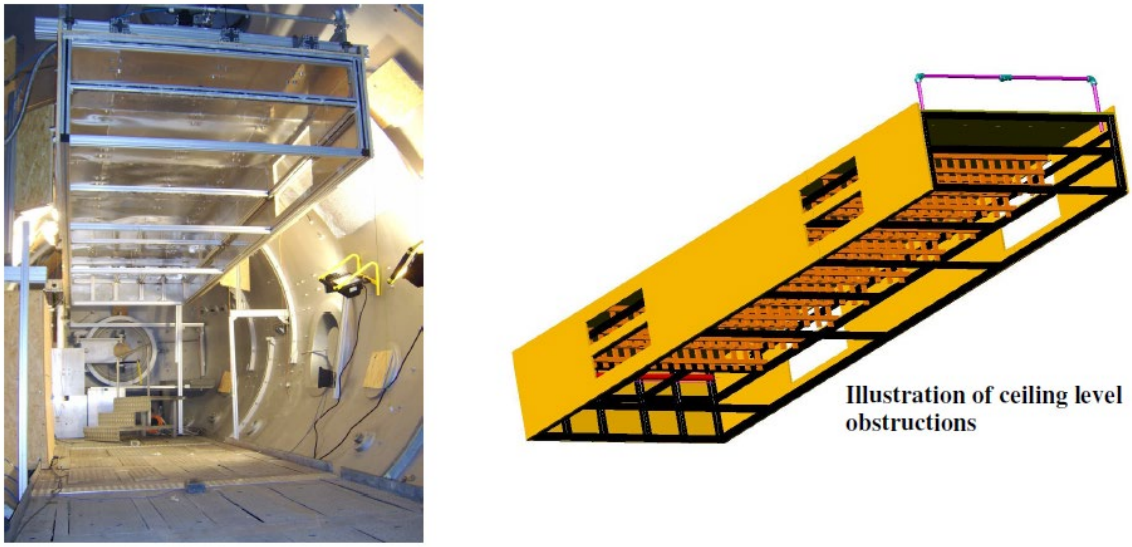

Figure 10: Experimental Setup for Deflagration Experiments (from [45])

In the set of experiments with no obstacles, slow flame propagation regimes were observed. The experiments with obstacles showed three distinct combustion regimes. The obstructions in the ceiling may have added turbulence to the flame propagation, which would make the explosions more severe. These results indicate that ceiling design and mitigation measures in tunnels are important which can be understood in the volume and layer height matrix shown in Figure 11 [45].

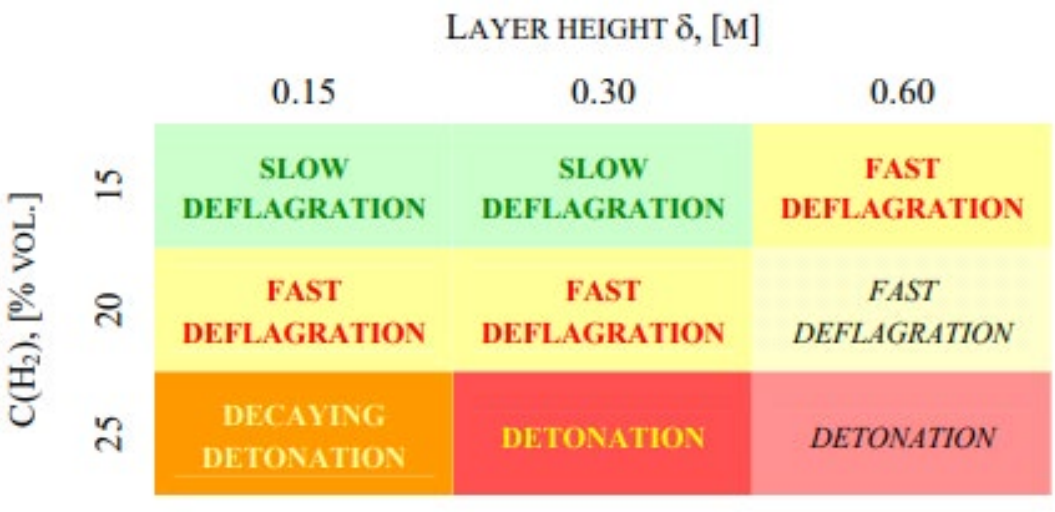

Figure 11: Concentration and Layer Height Effect on Combustion (from [45])

3.1.6. Fire experiments of carrier loaded FCEV in full-scale model tunnel

A series of fire experiments and numerical simulations of a carrier loaded with hydrogen FCEVs in a full-scale tunnel were conducted to calculate heat release and smoke generation rates by Seike et al. [46]. As shown in Figure 12, the experimental tunnel is 80 m long, 12.4 m wide, and 7.36 m wide with a horseshoe cross-section. The total HRR of the carrier loaded with hydrogen FCEVs was determined from the experimentally obtained temperature variation near the fire [46].

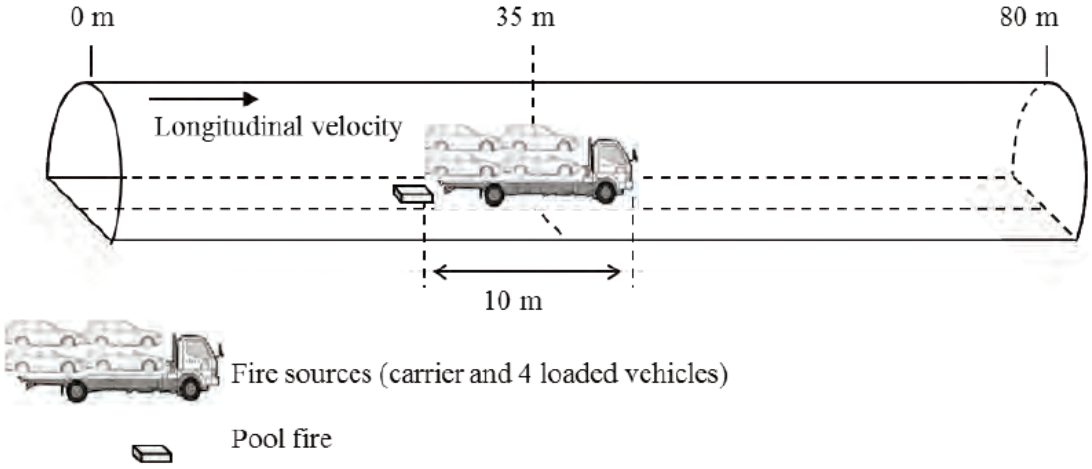

Figure 12: Experimental Tunnel Configuration and Carrier (from [46])

The total HRR was also estimated through numerical simulation. The individual HRR of each part of the car was calculated and summed to determine the total HRR. The different parts of concern were the carried vehicles without fuel, the hydrogen fuel which was approximately 17.6 m^3 of low-pressure hydrogen and another case of 43.6 m^3 of high-pressure hydrogen, the rear wheels, the driver's seat in the carrier vehicle, and a 1 m^2 gasoline pool fire. The methodology of estimating the HRR of each part and superimposing them to obtain the total HRR was then compared to the experimental results. As shown in Figure 13, for a vehicle containing 43.6 m^3 of compressed hydrogen, the numerical method and experimental results are in fairly good agreement [46].

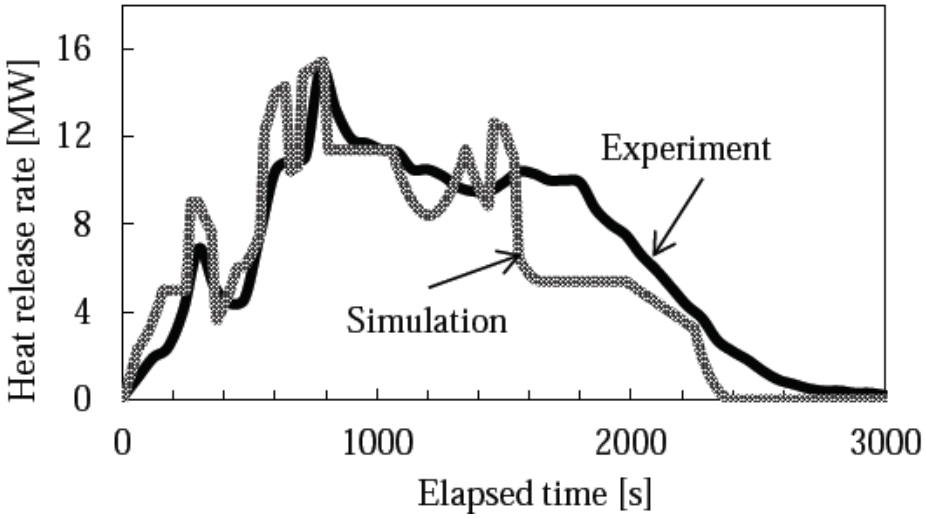

Figure 13: Comparison of Experimental & Simulated HRR for High Pressure Case (from [46])

This methodology was extended to predict the HRR of a carrier loaded with eight hydrogen FCEVs. It was determined that, when compared to a large bus fire, the HRR was larger after 10 minutes and the maximum HRR was 1.5 times greater [46].

3.1.7. Vapor Cloud Explosions from Ignition of Gaseous Mixtures in a Congested Region

A series of studies were carried out by Royle et al. [47] to measure the overpressure produced from methane and methane/hydrogen mixtures premixed with air when ignited within congested spaces. The experimental space was a 3 x 3 x 2 m region containing multiple layers of pipes. An image of the congested region is shown in Figure 14. A concrete wall sits adjacent to the one side of the congested region. The wall is positioned there to protect the control room and has been shown to not interfere with free field overpressure [47]. Additionally, the wall has embedded pressure sensors at different heights. For this series of experiments, the blockage ratio was reported as 4.40% the total volume. The outside of the grid was covered in a 23 μm thin plastic film which contained the gas prior to ignition. The plastic film was used only to contain the premixed gas mixtures prior to combustion and did not significantly restrict the outflow of gas or the pressure wave.

Figure 14: Congestion region or grid where gas was filled then ignited (from [47])

Hydrogen gas was mixed with air to form a stoichiometric ratio of 1.2 which reportedly produces the highest overpressures. Other gases evaluated in this study were mixtures of methane, air, and hydrogen which are all included in some of the figures and tables below. For this section, only results pertaining to hydrogen alone are discussed.

The ignition source was located at a height of 0.5 m off the ground and positioned at the center of the grid. For ignition, a 2.25 J capacitor was discharged through a spark gap of 6 mm. It was noted that the spark exhibited lower energy than what was discharged from the capacitor. For the instrumentation, overpressure values were measured by an array of low- and high-pressure pressure sensors. The location of the pressure sensors can be seen in Figure 15. All pressure sensors were positioned 500 mm above the ground except for the far field pressure sensors, which were mounted at higher locations due to the topology of the testing pad.

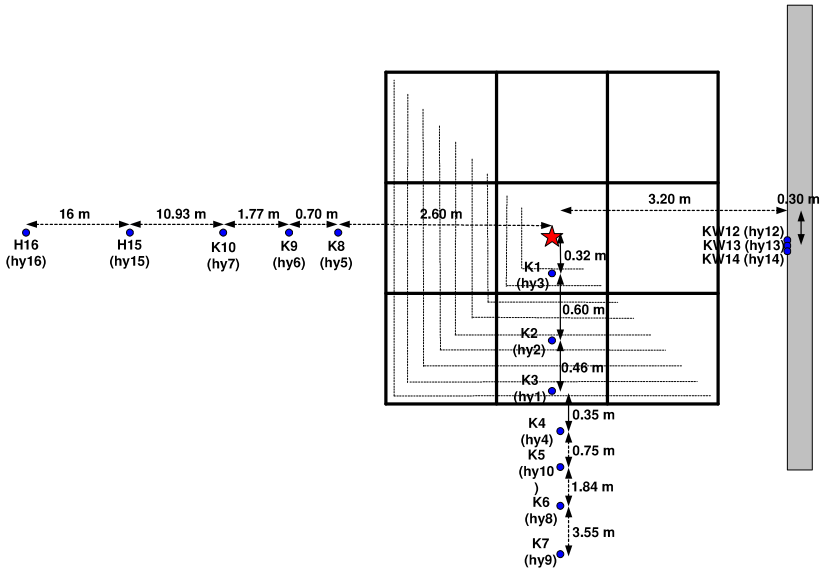

Figure 15: Pressure Sensors distributed in and around grid structure (from [47])

Pressures were measured across a wide span of locations including up the adjacent wall.

Table 9 lists the initial conditions prior to ignition. The pure hydrogen is labeled as NatHy_01. For the results of hydrogen/methane mixture experiments, we refer the reader to the paper [47].

Table 9: Initial Conditions of Experiment (from [47])

Measurement	Test Conditions: NatHy_01
Hydrogen (vol. %)	100
Number of Layers	9
Free Volume	17.207
Gas mixture temperature (°C)	11.0
Relative Humidity (%)	30.7
Atmospheric Pressure (kPa)	97.72
Mean Oxygen Concentration (%)	13.59
Partial Oxygen Pressure (kPa)	0.1359
Partial Nitrogen Pressure (kPa)	0.5127
Partial Water Vapor Pressure (kPa)	0.0041
Partial Fuel Gas Pressure (kPa)	0.3474
Mass of Hydrogen (kg)	0.498

It was noted that during the experiment the humidity was uncontrolled but was assumed to have a minor effect on the resultant explosion overpressure values. Figure 16 displays an image of the explosion immediately after ignition.

Figure 16: Image of pure methane combustion right after ignition (from [47])

Figure 17 and Figure 18 show the measured overpressure values at various locations for all mixtures. Recall that NatHy_01 corresponds to the hydrogen gas. Pressures were reported in the near-field (within and just outside of the grid) and far-field (further out from the grid) regions.

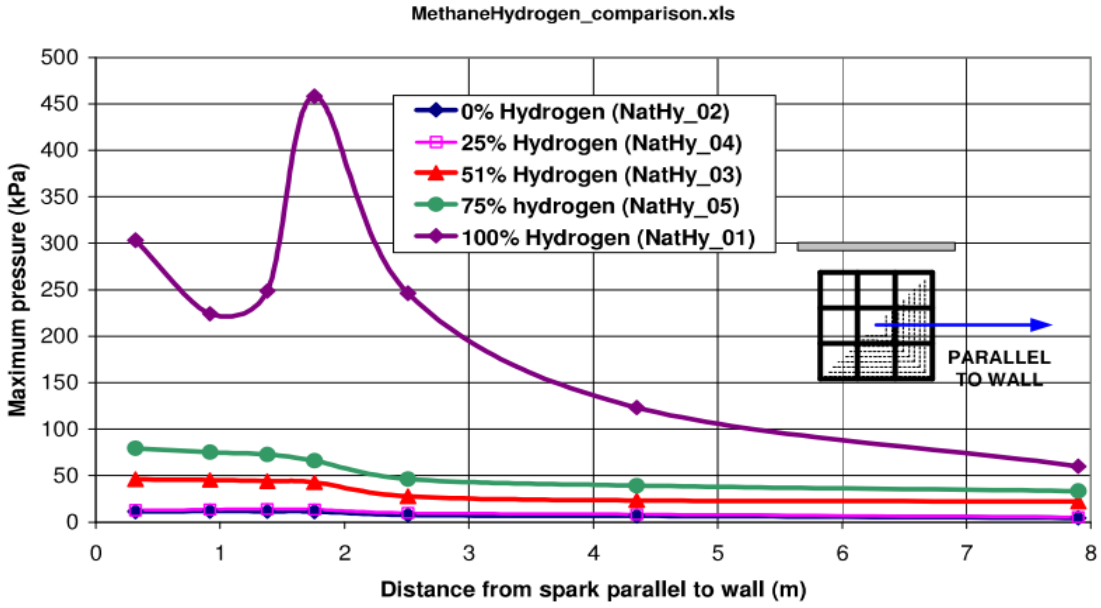

Figure 17: Overpressure vs. of distance parallel to the wall in the near field region (from [47])

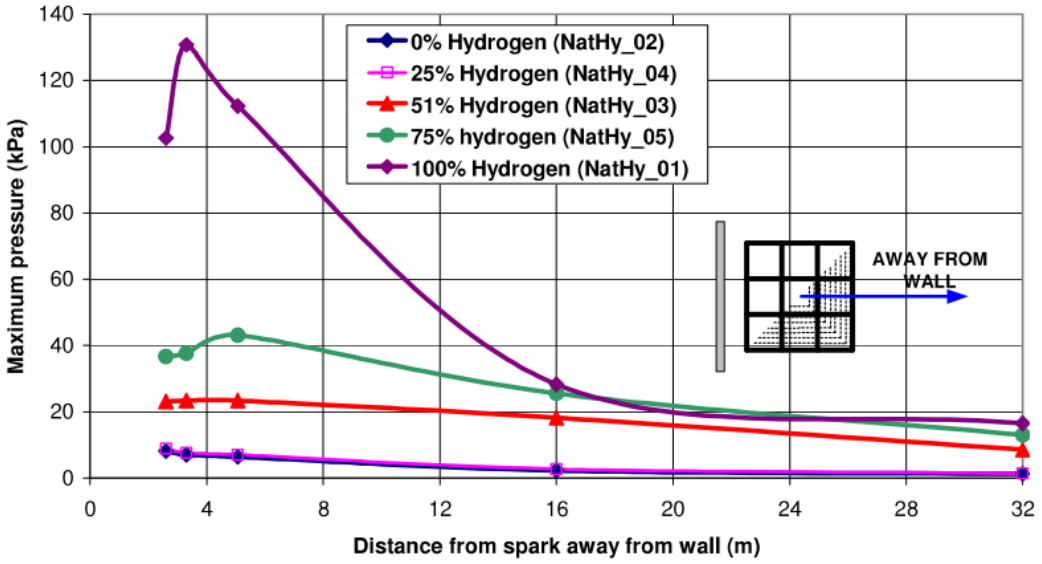

Figure 18: Overpressure vs. distance perpendicular to the wall in the far field region (from [47])

In the near field, values were well over 100 kPa and up to 450 kPa based on the distance parallel to the wall. At 32 m away, the overpressure drops to less than 20 kPa in the perpendicular direction and just above 50 kPa in the parallel direction. Referring to Table 1, 100 kPa is the fatality threshold for direct blast effects. Anything above 200 kPa has a 99% probability of fatality from direct blast effects. Note that this experiment represented the ignition of a pre-mixed 18 m^3 region with a high level of congestion— both the stoichiometric mixture size and level of congestion are probably unlikely to occur in a tunnel, especially simultaneously.

3.2. Modeling

A series of modeling efforts have been undertaken to understand hydrogen dispersion, deflagration, and hydrogen jet flame hazard in tunnels. Modeling was used to support a risk analysis of a hydrogen FCEV accident in a tunnel. The objective of the modeling was to predict the thermal expansion of the structural members and the temperature of the epoxy when a hydrogen jet flame impinges on the suspended tunnel ceiling (see Section 3.2.1). Furthermore, a CFD evaluation showed that the flame resulting from hydrogen release had the potential to damage tunnel equipment and structure (see Section 3.2.6). In another study, CFD modeling was performed in support of the evaluation of explosion risk of hydrogen vehicles (both cars and buses). A dispersion analysis determined realistic cloud sizes and hydrogen concentrations expected after a tunnel accident of various hydrogen vehicles (assuming delayed ignition). It was determined that the resulting overpressure is insignificant in terms of risk to human life (see Section 3.2.2). Another effort involved a turbulence modeling study evaluating hydrogen release and combustion, variable tunnel ventilation, and variable delayed ignition time. These results showed that larger ventilation rates decreased the growth rate of overpressure after ignition and the attenuation rate after reaching the peak while increased ignition time delay had the opposite effect (see Section 3.2.5). Also, a series of CFD simulations were performed to evaluate diffusion of leaked hydrogen in tunnels. These simulations showed that in tunnels without ventilation, the geometry effects the hydrogen diffusion (see Section 3.2.7). Finally, CFD models of hydrogen deflagration in a tunnel were compared with the results from experiments to validate the results of the CFD code (see Section 3.2.3 and 3.2.4).

3.2.1. Hydrogen FCEV Tunnel Safety Study

CFD, heat transfer, and solid mechanics modeling was performed by Sandia National Laboratories [48] in support of the risk analysis of a hydrogen FCEV accident in a tunnel. The scenario modeled in support of the risk analysis was a hydrogen vehicle in an accident exposed to a resulting fire (see Section 3.3.1 for additional details).

The objective of the modeling was to predict the thermal expansion of the structural members and the temperature of the epoxy when a hydrogen jet flame impinges on the tunnel ceiling. The analysis was divided into three parts: 1) a CFD simulation of the flame, 2) a heat transfer simulation of the structural members, and 3) a solid mechanics analysis of the structural members. A Sandia-developed code called Sierra was used to perform the simulations. Sierra is divided into different modules that can interact with each other. The Fuego module was used for the CFD simulation, the Aria module was used for the heat transfer model, and the Adagio module was used to calculate the deflection of the structural members. The CFD simulation provided the boundary conditions for the heat transfer simulation, specifically the radiative and convective heat flux on the tunnel ceiling. Note that due to computational limitations, the smallest reasonable tank orifice diameter that can be modeled is 5.25 cm. This is conservative because the velocity was kept constant for the larger diameter, so the mass flow and total heat release are larger than what is expected for the realistic 2.25 mm tank orifice diameter. While the velocity could be decreased in order to compensate for the larger release diameter, the flame impingement would be underestimated [48].

These boundary conditions served as input to Aria to calculate the temperature profiles across the structural members. Specifically, the reference temperature, heat transfer coefficient, and the irradiation from the CFD model were used as boundary conditions on the surface in direct contact with the heated gases. The temperature profiles on the structural members were input into Adagio to calculate the deflection due to thermal strain on each structural member. A simplified analysis was also performed to determine if the stainless-steel hangers can hold the concrete panels when the hydrogen jet is impinging the stainless-steel bar surface. Note that the different tunnel structures (Central Artery North Area or CANA tunnel and Ted Williams Tunnel) were each evaluated with and without ventilation [48].

Table 10 shows a summary of the maximum temperature and deflection for the CANA and Ted Williams (TW) structures. The worst-case scenarios were seen when the ventilation is not operating. Both the CANA and Ted Williams Tunnel results show that the thermal conditions may result in localized concrete spalling in the area where the hydrogen jet flame impinges the ceiling. If the ventilation is operating, the maximum temperature is significantly lower, and spalling is not expected to occur. The total stress on the steel structure was significantly lower than the yield stress of stainless steel and ASTM A36 at the maximum steel temperature even when the ventilation was not on. Therefore, the steel structure is not expected to be compromised. Also, the epoxy remains at ambient temperature and so should not degrade or fail due to this exposure. The maximum deflection of the steel hanger is 7 mm, which will not impact the structural integrity of the beam. Note that several conservative assumptions were made in this modeling, so the temperature observed should be lower than what which results in spalling [38]. Table 10 shows the results of the modeling. Each jet flame fire curve is created with ventilation (V) and without ventilation (NV).

Table 10: Results Summary of Hydrogen FCEV in Tunnels Risk Modeling (from [48])

Fire Curve		Maximum Temperature (°C)	Maximum Deflection (mm)	Yield Stress (MPa)
Hydrocarbon		~750	~5	-
ISO 834		~750	~10	-
H_2 Jet Flame CANA (NV)		592	19.4	-
H_2 Jet Flame CANA (V)		336	7.6	-
H_2 Jet Flame TW (NV)	Concrete	1,088	<200	-
	Stainless Steel	706	~7	147.79
	ASTM A36	-	-	399.9
H_2 Jet Flame TW (V)	Concrete	805	43.5	-
	Stainless Steel	436	1.3	214.76
	ASTM A36	-	-	172.37

3.2.2. Hydrogen Vehicle Explosion Risk in Tunnels

CFD modeling was performed by Middha and Hansen [49] in support of the evaluation of explosion risk of hydrogen vehicles (both cars and buses) in a tunnel (see Section 3.3.2 for additional details) [49]. The objective of the modeling was to predict a quantitative explosion risk for hydrogen vehicles in tunnels. All the scenarios described in Section 3.3.2 were evaluated using the CFD code FLACS. Both NGV and H2 vehicles were studied in the simulations but this section will only comment on results pertaining to H_2. The H_2 car and bus parameters are described by Middha and Hansen as follows:

1. Compressed hydrogen gas city bus with 40 kg H_2 stored in 8 cylinders (two sets of 4 each) – 5 kg per cylinder at a storage pressure of 350 bar. The vehicle was represented as a rectangular block (12.0 m x 2.55 m x 2.9 m) with the distance to the top of the tanks being 3.1 m.
2. Compressed hydrogen gas car with 5 kg H_2 stored in 1 cylinder at a storage pressure of 700 bar. The car was represented as a simple rectangular block (5.0 m x 1.9 m x 1.5 m) located 0.3 m above the ground.

As for the tunnels, two different cross sections were evaluated, rectangle and horseshoe shape, see Figure 19 for cross-sectional dimensions. Both tunnels were modeled with a length of 500 m.

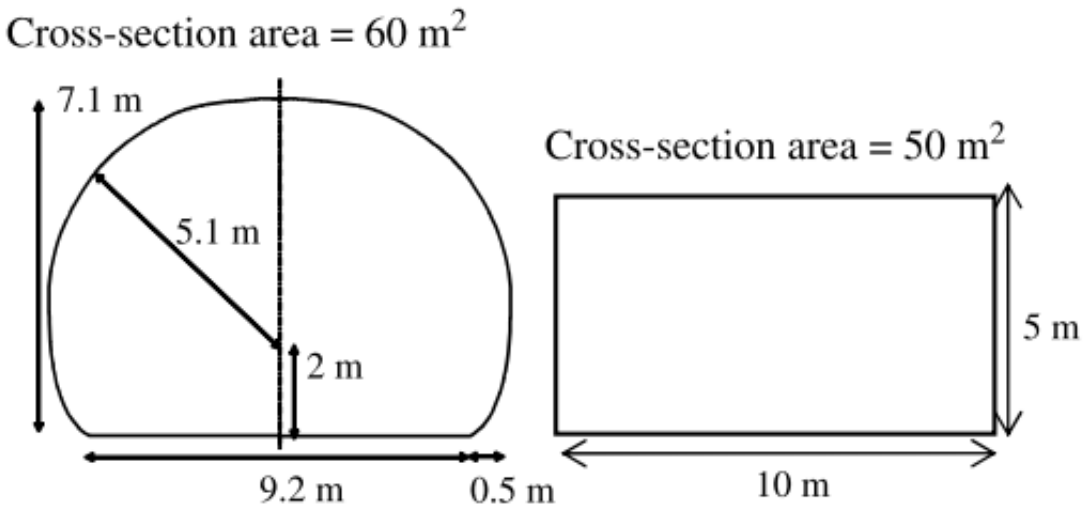

Figure 19: Tunnel cross-sectional dimensions (from [49])

In addition to the cross-sectional dimensions and length, the geometry of the modeled tunnel included vehicles. The tunnels were dual lane with traffic running a single direction. The tunnel was assumed to be full of cars and buses spaced out evenly by 1.5 m. The vehicle distribution was a repeated pattern of six cars follow by one bus. The vehicles were placed such that one bus and one car were at the exact center length wise of the tunnel in separate lanes. The same geometry was used for both the car and bus release. The releases were assumed to be choked flow. The mass flow rate of the H_2 for choked flow at 350 and 700 bar is displayed in Figure 20. Note that this was computed assuming a discharge coefficient of 0.8 and a 4 mm opening.

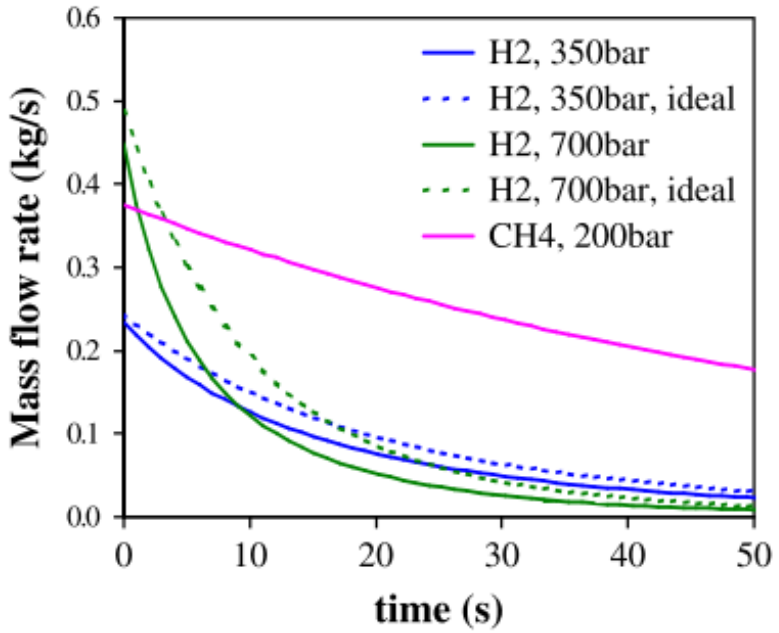

Figure 20: Mass flow of release for CNG and various H2 simulations (from [49])

Ignition points were varied from the center of the vapor cloud to the outer edges (length wise of the tunnel). Ventilation velocities were also varied between the models.

A dispersion model simulating the release of the fuel systems was carried out. Table 11 lists the maximum flammable gas cloud size for each configuration as well as the equivalent stoichiometric cloud or the Q9 quiescent cloud. This is a scaled smaller stoichiometric gas cloud that represents the same explosion load as the non-homogenous larger cloud. It is scaled based off the weighted volume expansion, flammable volume, and laminar burning velocity. The flammable cloud and its stoichiometric and Q9 equivalents along with the maximum pressures for the combustion of the flammable gas clouds are listed in Table 11 below:

Table 11: Summary of gas cloud & overpressure for various vehicles in both tunnels (from [49])

Vehicle/Release Characteristics	Inventory (kg)	Maximum flammable gas cloud size in m^3 (kg)		Maximum equivalent stoichiometric flammable gas cloud size in m^3 (kg)		Max. pressure for max. equiv. cloud Q9 Quiescent/Pre-ignition turb.	
		Horseshoe Tunnel	Rectangular Tunnel	Horseshoe Tunnel	Rectangular Tunnel	Maximum Q9 Equivalent Volume (m^3)	Maximum overpressure (barg)
Car LH2	10	1.4 (0.007)	1.8 (0.009)	0.02 (0.003)	0.02 (0.004)	0.0	<0.05/0.1
Car H2 Gas 700 bar (vent up)	5	281 (1.14)	273 (1.21)	4.42 (0.07)	4.31 (0.09)	4.4	0.05/0.10
Car H2 Gas 700 bar (vent down)	5	268 (1.33)	308 (1.39)	17.75 (0.29)	8.77 (0.18)	17.8	0.11/0.34
Bus H2 Gas 350 bar	5	213 (0.89)	190 (0.81)	2.16 (0.04)	1.94 (0.04)	2.2	0.05/0.10
Bus H2 Gas 350 bar	20	1795 (7.46)	3037 (13.97)	27.46 (0.45)	24.67 (0.49)	27.5	0.11/0.34

From the coupled dispersion combustion simulations, it is predicted that overpressure values can produce minor damage to people and property within the tunnel. The data presented in Table 11 were combined to create a frequency of exceedance curve for overpressures during combustion of gaseous hydrogen clouds, shown in Figure 21. Overpressure values outside the hazardous range (less than 0.1 barg) are much more likely than higher overpressures that can be hazardous to tunnel occupants. This is important information to perform a risk analysis, but the method used to create the exceedance curves is not discussed in detail.

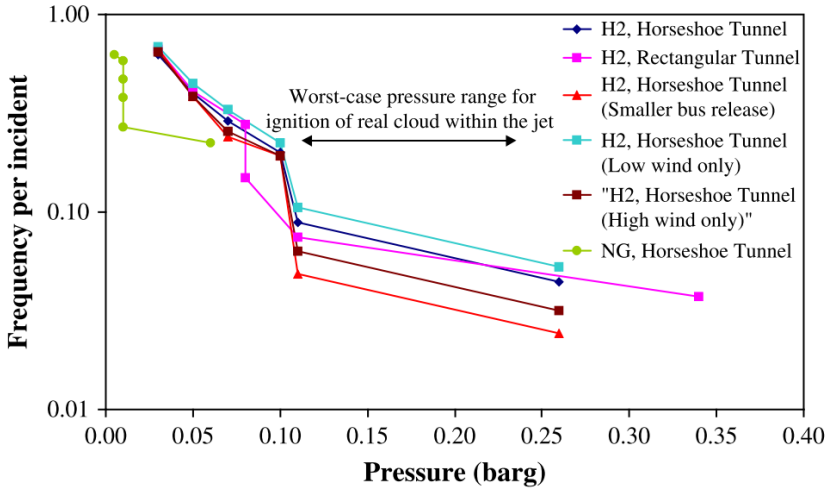

Figure 21: Exceedance curves for overpressure values per fuel type (from [49])

3.2.3. CFD Modeling of Hydrogen Deflagration in a Tunnel

Deflagration in homogenous, near stoichiometric hydrogen/air mixtures in a model of a tunnel were simulated through CFD modeling techniques by Tolias et al. [50]. The ADREA-HF CFD code was used for this modeling. The purpose of this modeling was to baseline the results from the ADREA-HF CFD code with that of the experiment discussed in Section 3.1.2. Specifically, the time-dependent overpressure data generated from the CFD modeling was compared directly with the experimental data. The two cases that were examined were the empty tunnel and tunnel with simulated traffic with a homogeneous hydrogen/air mixture with a 30% hydrogen concentration by volume. While this experiment used this concentration for each scenario, more plausible concentration would need to be used in future work. Figure 23 shows the experimental and computational overpressure results at different locations along the tunnel. As shown, the computational results are in general agreement with the results of the experiment. Therefore, the CFD code was able to simulate the combustion process and estimate the resulting overpressures.

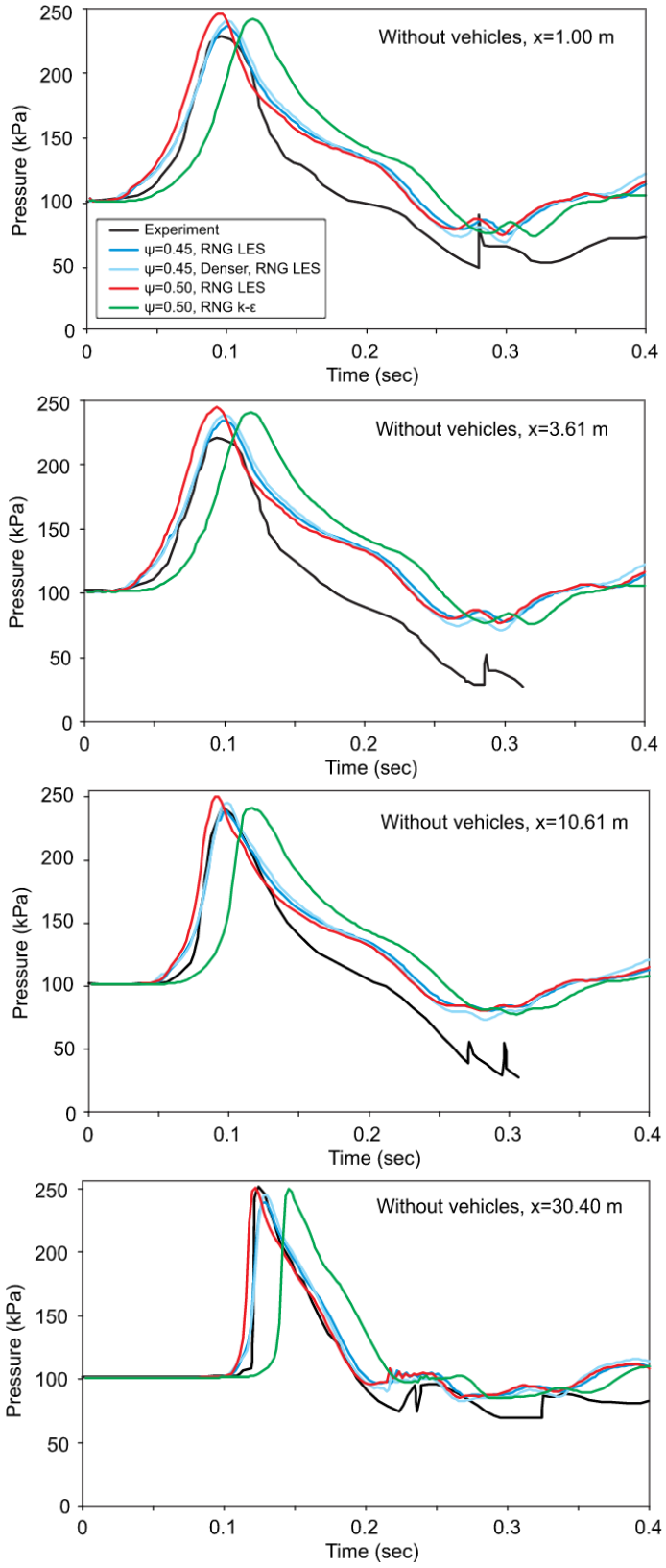

Figure 22: Overpressure Results without Vehicles (from [50])

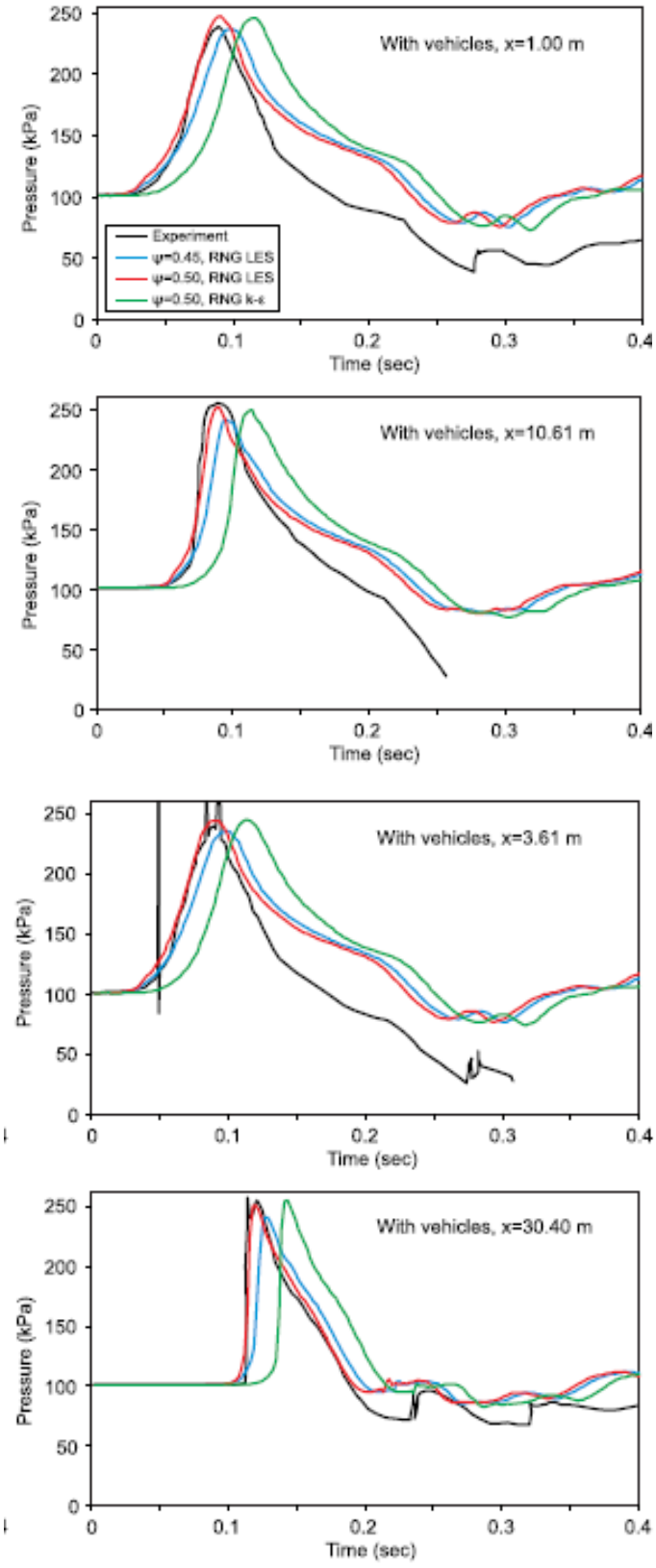

Figure 23: Overpressure Results with Vehicles (from [50])

3.2.4. Releases from Hydrogen Fuel-cell Vehicles in Tunnels

Houf et al. [51] modeled the consequence of hydrogen TPRDs being activated, the flammable gas venting to the environment, and the time-delay to ignition within a tunnel. Multiple simulation tools were used to perform the evaluation. To model the TPRD releases inside ventilated tunnels, Sandia's computational fluid mechanics code, Fuego, was used. An FCEV was modeled with three separate tanks, each containing 1.67 kg of hydrogen at 70 MPa. For these simulations, high-pressure hydrogen gas was vented simultaneously from three separate onboard tanks through three separate TPRD vents located on the bottom of the FCEV. Figure 24 shows a diagram of the tunnel model layout with transverse ventilation. The evolution of the hydrogen/air mixture was modeled after blowdown from the TPRDs on the FCEV. A Sandia developed code, NETFLOW, was used to model the transient nature of the tank blowdown [51].

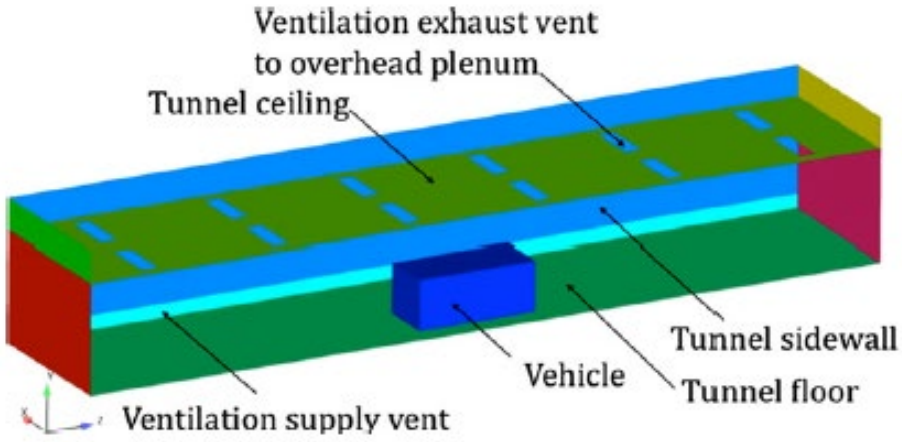

Figure 24: Tunnel Model with Transverse Ventilation (from [51])

Figure 25 shows the simulation results of the hydrogen release and mixing in the tunnel model. Note that the solid lines are the total flammable volume in both the tunnel and ventilation plenum, and the dashed lines represent the flammable volume in the ventilation plenum only. As shown, a range of ventilation rates were evaluated, and the flammable volume decreases with increasing ventilation rate. Also, the flammable volume disperses quicker with a higher ventilation rate [51].

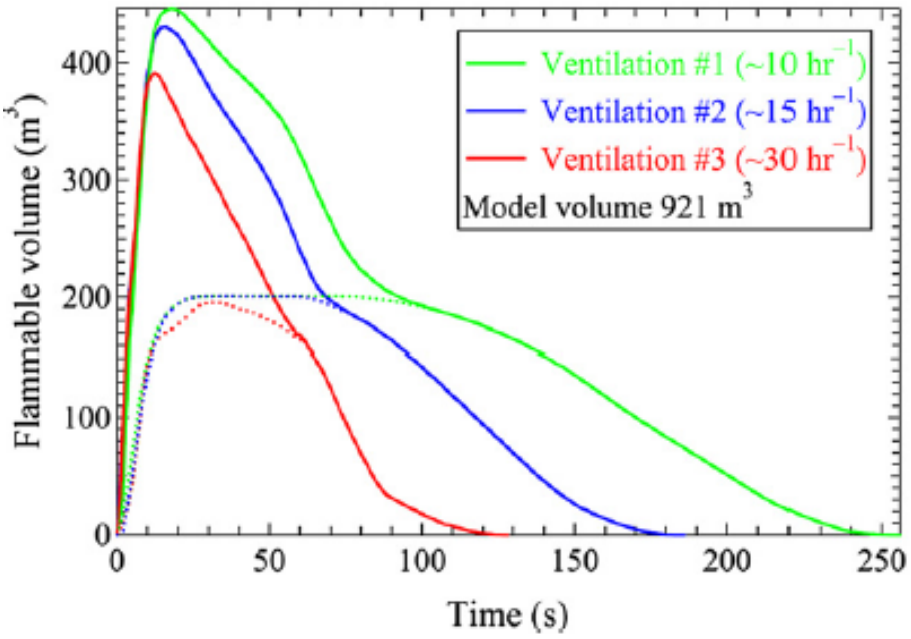

Figure 25: Simulation Results Showing Evolution of Flammable Hydrogen Volume (from [51])

A FLACS model was developed to perform ignition overpressure simulations for the simulations evaluated in Fuego. Figure 26 shows the results from the simulation modeling at different ignition times and locations of the ignition source after the beginning of the TPRD release. As shown, overpressure peaks at an ignition delay of around 5 seconds [51]. Referring to Table 1, ignition delays of about 4 to 8 seconds result in overpressures approaching or above the fatality threshold level. These results show the importance and sensitivity to various ignition locations and delays.

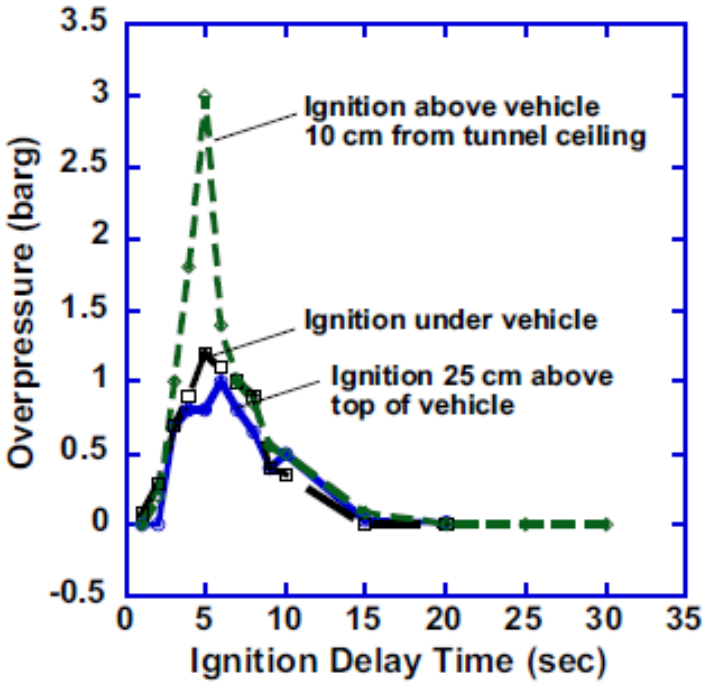

Figure 26: Simulation of Peak Ignition Overpressures vs. Ignition Delay (from [51])

3.2.5. Hydrogen Release and Combustion in Subsea Tunnels

Turbulence modeling was used to evaluate hydrogen release events from vehicles in subsea tunnels by Bie and Hao [52]. As part of this study, variable tunnel ventilation conditions and the resulting hydrogen cloud sizes, as well as delay in ignition time, were assessed to fully characterize this risk. The partially averaged Navier-Stokes turbulence model was used to research the hydrogen release and combustion phenomena as it related to the risk inside highway tunnels. The physical tunnel used as the basis of this modeling effort was the Bay subsea tunnel, a three-lane highway. The model of the tunnel was 13.5 meters wide, 5 m high, and 500 meters long. A typical mid-sized hydrogen FCEV was modeled containing 4.955 kg H_2 at 70 MPa. Varying ventilation conditions of 0 m/s (no ventilation), 1 m/s, 3 m/s, and 6 m/s were evaluated with five monitoring points spaced at 5 meter horizontal intervals (see Figure 27) [52].

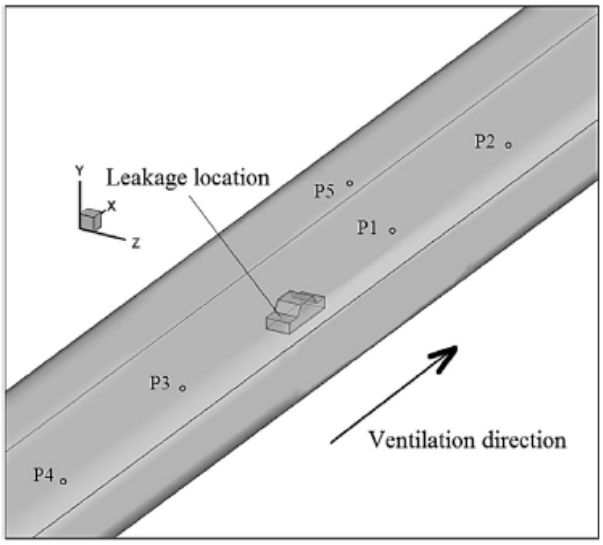

Figure 27: Subsea Tunnel Model with FCEV and Monitoring Points (from [52])

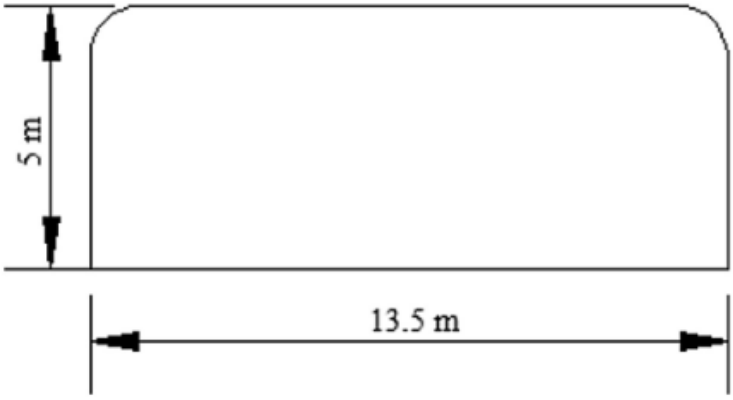

Figure 28: Subsea Tunnel Model Cross Section (from [52]

Figure 29 and Figure 30 show the longitudinal and traverse hydrogen concentration contours at three seconds after event initiation for different ventilation conditions. As shown, the ventilation rate has a significant influence on the hydrogen distribution after the TPRD release event. The

upstream monitoring points showed less hazardous concentrations of hydrogen than the downstream monitoring points [52].

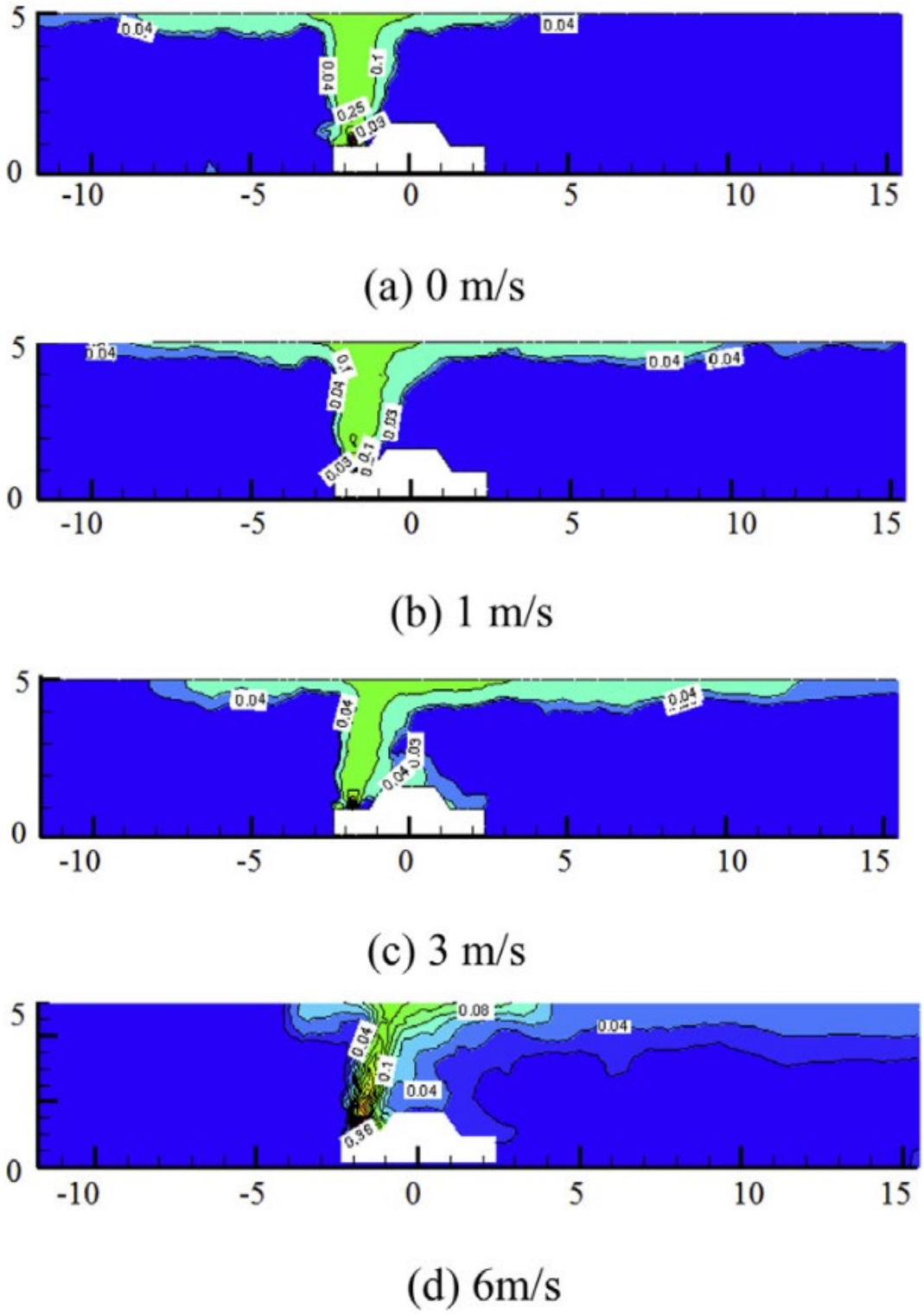

Figure 29: Longitudinal H2 Distribution Various Ventilation Conditions (from [52])

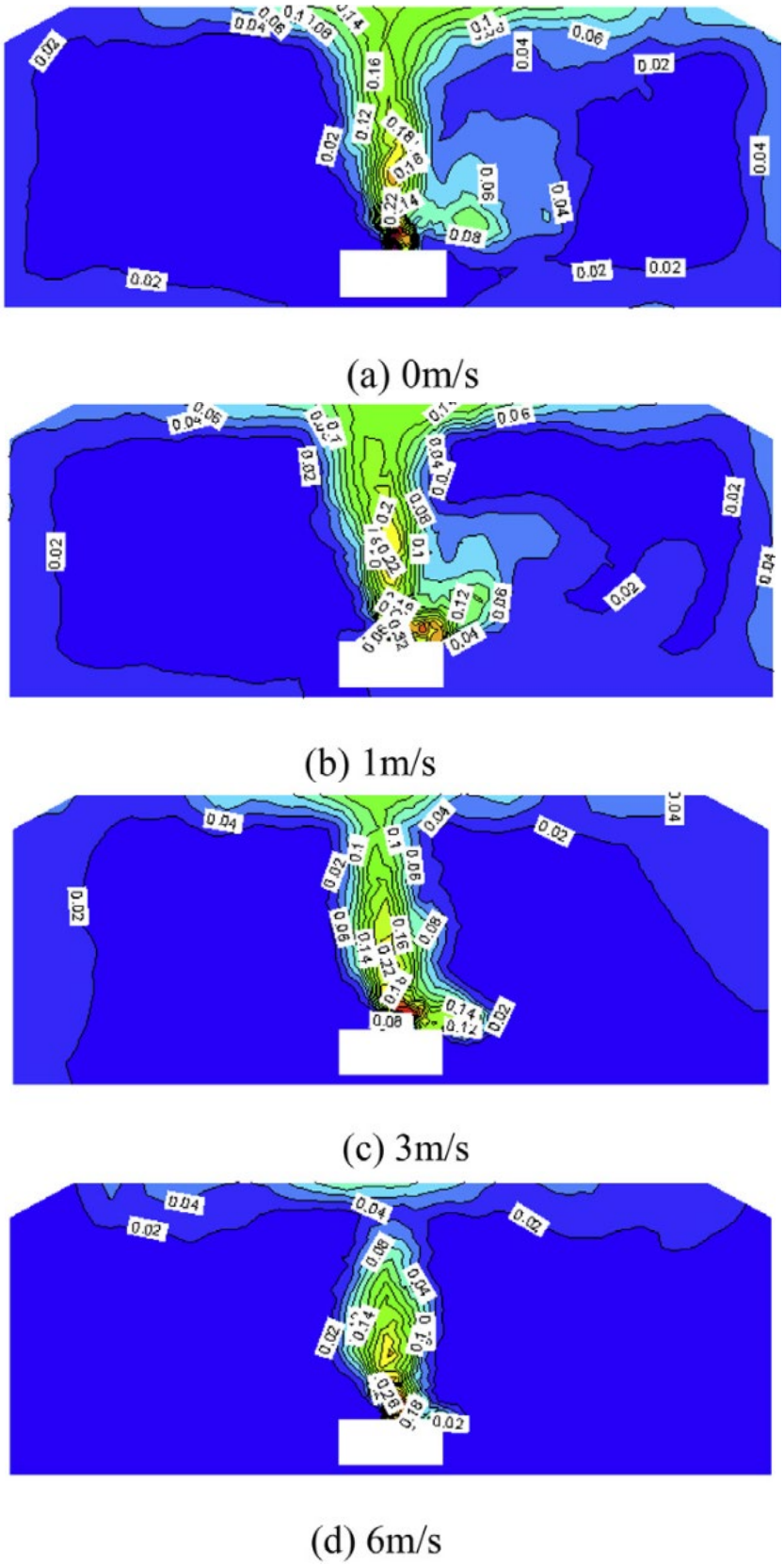

Figure 30: Traverse H2 Distribution Various Ventilation Conditions (from [52])

Figure 31 and Figure 32 show the overpressure history for different ventilation conditions at ignition times of 3.1 s and 6.1 s, respectively. There are four monitoring points (P1, P2, P3, and P4) that measure the overpressure. P1 was arranged 5 m away from the leakage location along the direction of traffic, P2 was arranged 10 m away from the leakage location along the direction of traffic, P3 was arranged 5 m away from the leakage location in the inverse direction of vehicle, and P4 was arranged 10 m away from the leakage location in the inverse direction of vehicle per Bie and Hao [52]. The literature specifies that P1 and P2 are downstream, while P3 and P4 are upstream [52].

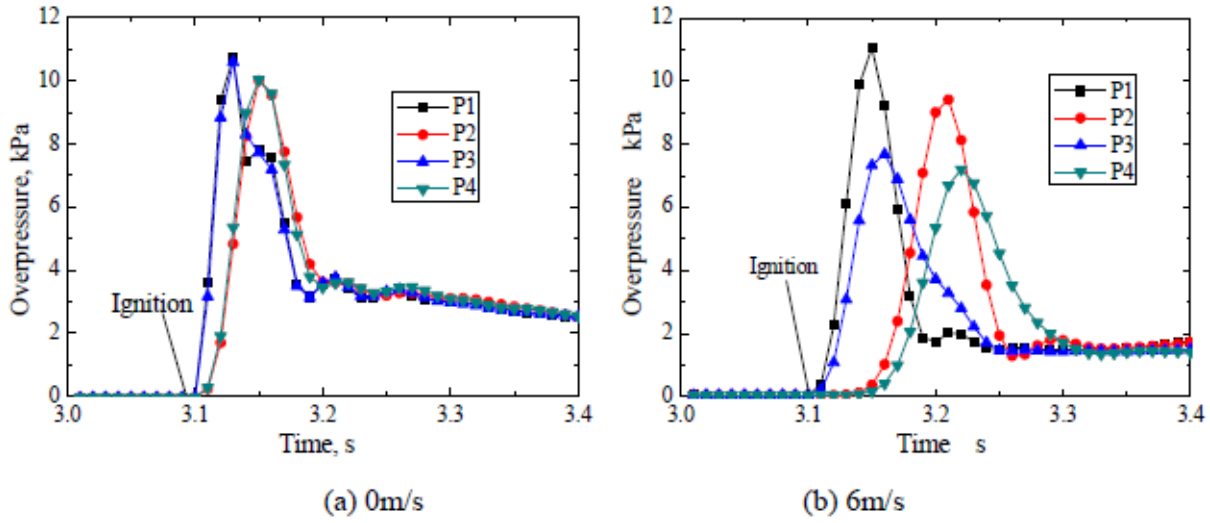

Figure 31: Overpressure History at Ignition Time of 3.1 Seconds (from [52])

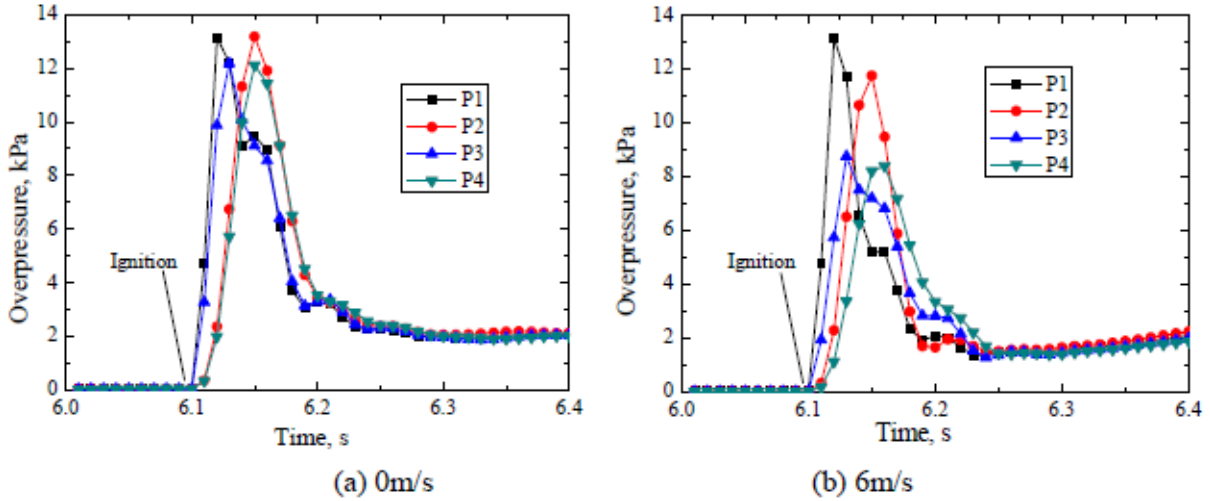

Figure 32: Overpressure History at Ignition Time of 6.1 Seconds (from [52])

The overpressure shown in Figure 31 and Figure 32 shows the peak overpressures for the upstream locations (P3 & P4) are appreciably reduced with ventilation from 10-12 kPa at 3.1 seconds down to 7.5-8 kPa and 12 kPa down to 9 kPa at 6.1 seconds. Only P2 downstream shows a small reduction in the overpressure measured comparing with and without ventilation.

3.2.6. Hydrogen Jet Flame Hazard in Tunnels

An evaluation of the possible fire scenarios of hydrogen cars in tunnels was conducted to assess the implications on a tunnel ventilation system. To accomplish this, CFD simulations were evaluated on a tunnel with a length of 102 m and a cross-section of 5 m by 5 m. FLUENT was used to simulate the smoke flow in the tunnels after a fire. Figure 33 shows the tunnel geometry and boundary conditions of the CFD case. As shown, the hydrogen FCEV is located 40 m from the air inlet [53].

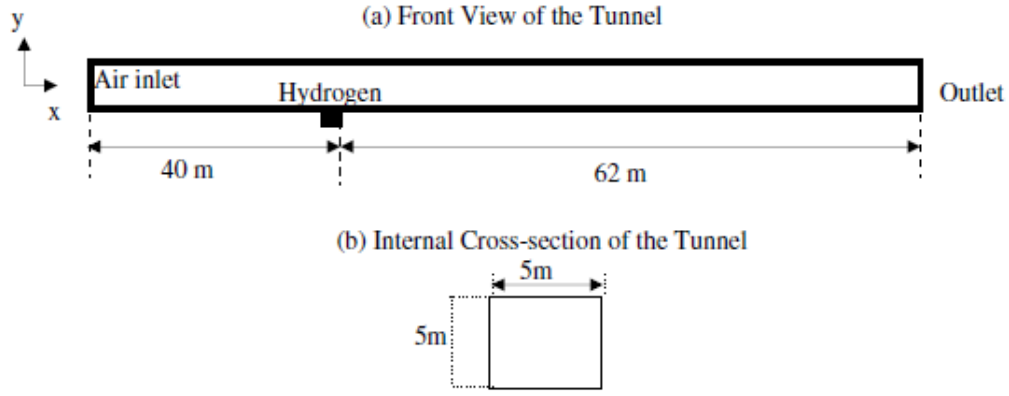

Figure 33: Tunnel geometry and Boundary Conditions of CFD Model (from [53])

Two scenarios were evaluated: a) 6 MW hydrogen fire with 2.5 m/s ventilation, and b) 30 MW hydrogen fire with 2.5 m/s ventilation. This study selected these two specific scenarios based on realistic hydrogen release conditions from a hydrogen car. Hydrogen was released at a rate of 0.05 kg/s and at a velocity of 10 m/s which resulted in a 6 MW hydrogen fire lasting about 1 minute in the first scenario. In the second scenario, hydrogen was released at a rate of 0.25 kg/s and a velocity of 50 m/s, which resulted in a 30 MW fire for a shorter duration. The results of the CFD evaluation show that the ventilation in the 6 MW fire can fully eliminate the back layering. However, this is not true of the 30 MW fire. Moreover, the 30 MW fire resulted in the flame reaching the tunnel ceiling and spreading under the ceiling for large distances. This could result in serious damage to the tunnel equipment and structures along the ceiling [53].

3.2.7. Diffusion of Leaked Hydrogen in Tunnels

A series of CFD simulations were performed to evaluate diffusion of leaked hydrogen in tunnels [54]. Multiple tunnels with variations in slope, leak location, cross-section geometry, ventilation rate, and ventilation type were evaluated for a 60 m^3 (unmixed, approximately 5 kg) hydrogen leak. In the vehicle tunnel simulations (Case A), a long model tunnel and an underwater model tunnel were evaluated. Figure 34 illustrates the differences between these tunnels. Each tunnel was evaluated with varying ventilation flow rates [54].

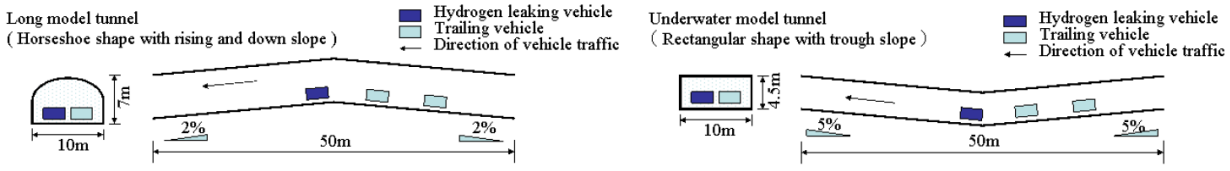

Figure 34: Case A Simulation Tunnel Geometries

The general flow modeling software code STAR-CD was used in the calculation model. It was found that in tunnels without ventilation, the geometry effects hydrogen diffusion. The slope of the long tunnel model resulted in hydrogen collecting in the tunnel for several dozen minutes. In tunnels with the underwater model tunnel slope, hydrogen is rapidly cleared from the tunnel. For each Case A tunnel geometry with ventilation, the hydrogen is removed by the ventilation flow within several dozen seconds. In the Case B simulations, there is a brief time in which hydrogen with a concentration at about LFL flows into the power collector. For the Case C simulations, there is no concern about inflow of hydrogen at concentrations greater than LFL since that time is very short [54].

Figure 35 illustrates the tunnel evaluated in the Case B simulations. In these simulations, an electrostatic dust collector is in a branch off the main tunnel. The location of the leaked hydrogen is varied [54].

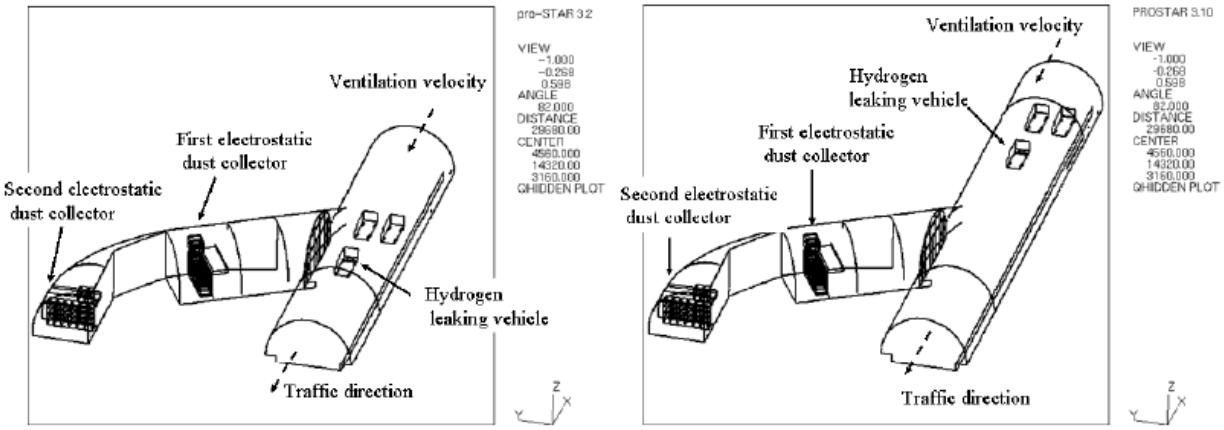

Figure 35: Case B Simulation Tunnel Geometry

Figure 36 illustrates the tunnel evaluated in the Case C simulations. In these simulations, an underground ventilation facility is in a branch off the main tunnel and air is released through a vertical shaft opening to the outside. The location of the leaked hydrogen is varied [54].

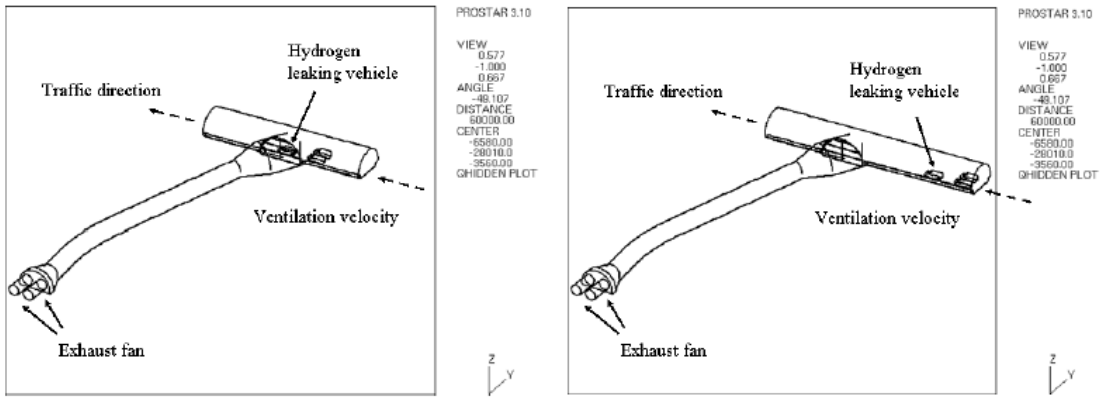

Figure 36: Case C Simulation Tunnel Geometry

3.2.8. Gaseous release, dispersion, and combustion for automotive scenarios

Venetsanos et al. [55] CFD was used to study the effects of a compressed gas release from a commercial vehicle in urban areas. One urban area simulated was a tunnel with a single deck city bus located centrally along the length. Variable releases from both hydrogen and CNG fuel tanks were evaluated. The fuel storage systems modeled represented that of a typical European bus with fuel containers located along the roof, forward from the midpoint. The system consisted of 2 sets of 4 tanks connected as displayed in Figure 37. The specific CFD solvers utilized were ADREA-HF for dispersion and REACFLOW for combustion.

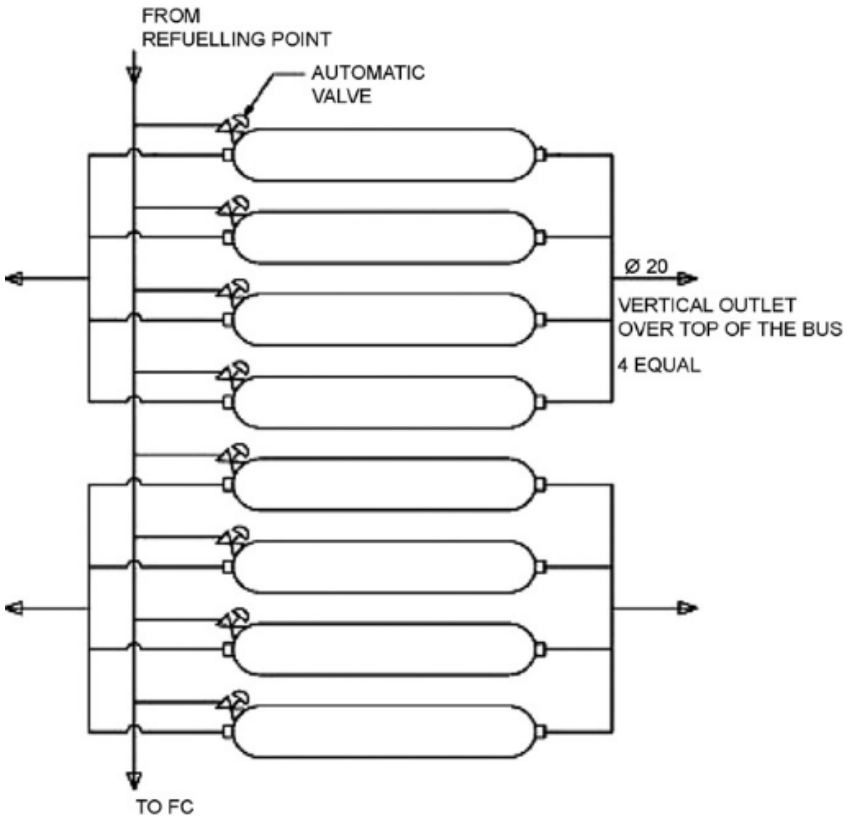

Figure 37: Fuel tanks configuration for both CNG and CH2 gas (from [55])

The tanks contained a total of 40 kg at 20, 35, and 70 MPa of H_2. This is representative of a standard CGH_2 bus and the 70 MPa case exceeds normal bus configurations. The main vent lines are controlled by thermally activated pressure relief devices (TPRD). As shown, each TPRD is attached to manifold connected to 4 tanks (2 TPRDs per set of 8 tanks). Multiple release scenarios were evaluated by varying TPRD orifice size and tank evacuations. A summation of storage parameters is shown in Table 12. Note this study and the figures below have results for hydrogen and methane.

Table 12: Storage Configurations Details (from [55])

Fuel	Pressure (MPa)	Fuel density at 15 °C (kg m^{-3})	Total storage volume (l)	Single cylinder volume (l)	Total fuel mass (in 8 cylinders) (kg)	Fuel mass in one cylinder (kg)
H_2	20	14.96	2672	334	40	5
H_2	35	24.02	1600	200	40	5
H_2	70	40.18	996	124.5	40	5
CH_4	20	168	1000	125	168	21

The computational domain was modeled as a tunnel of 212 m length with a cross-sectional area displayed in Figure 38. As mentioned, the bus was located along half the length of the tunnel in a centralized location. Besides the bus, the tunnel was assumed to be empty and the walls were modeled as smooth surfaces. Additionally, the air was assumed quiescent to represent a worst case scenario.

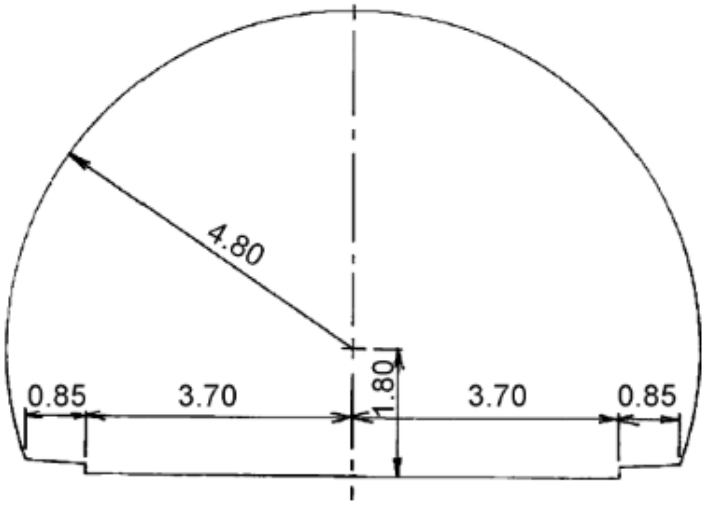

Figure 38: Tunnel Cross Section (from [55])

Two release cases were evaluated for CNG. Table 13 lists the descriptions of all cases, Case 1, and 3 were selected since Case 2 lies between them.

Table 13: Storage Configurations Cases (from [55])

Case no.	Possible release	Description	Gas released (kg)
1	Vehicle out of service (automatic valves closed) and one random PRD fuse fails open OR Fire causes a single PRD to trigger[a]	Gas from one cylinder released through 1 PRD vent and 1 outlet	Hydrogen—5 Natural gas—21
2	Vehicle in service (automatic valves open) and one random PRD fuse fails open OR Fire causes a single PRD to trigger[a]	Gas from all cylinders released through 1 outlet	Hydrogen—40 Natural gas—168
3	Fire causes all PRDs to trigger simultaneously[a]	Gas from all cylinders released through all 4 outlets	Hydrogen—40 Natural gas—168

[a]It is assumed that the fire does not ignite the gas. Anecdotal reports by various research and testing organizations indicate that fires that cause temperature triggered PRD to open may not immediately ignite the vented gas. The fire that triggers the thermally activated PRD may not be in a position that causes the vented gas to ignite, since the exit from the vent may not be situated in the fire.

The results for Case 1, where only one cylinder was released through a single TPRD, are shown in Figure 39. The left frame shows the flammable mass and the right frame the total available energy. The available energy was computed by multiplying the released mass of fuel by the lower heat of

combustion. The flammable mass was calculated from the amount of fuel/air mixture released which was within the FL. Figure 40 displays the results for case 3, where all 8 cylinders released through all 4 TPRDs simultaneously.

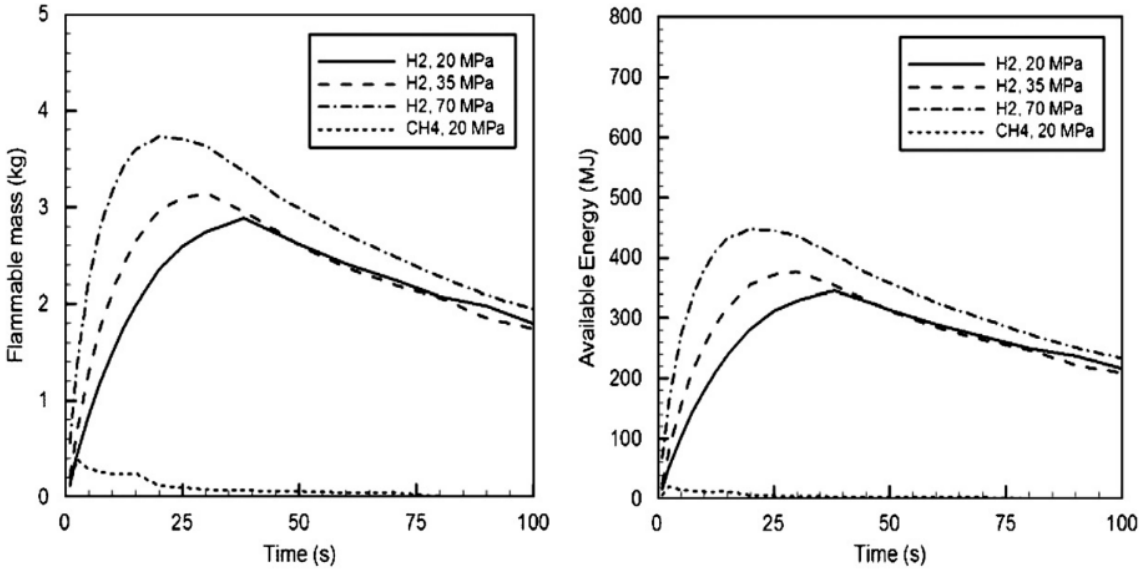

Figure 39: Flammable mass and available energy of released gas in Case 1 (from [55])

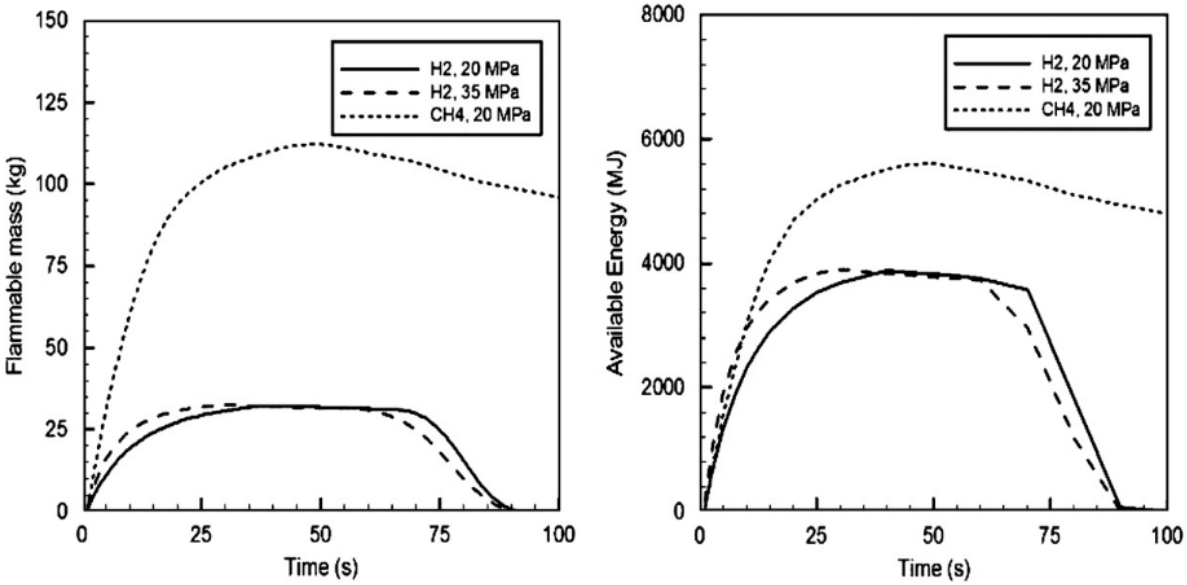

Figure 40: Flammable mass and available energy of released gases in Case 3 (from [55])

Note the change in scales between Figure 39 and Figure 40 For Case 1 both the flammable mass and available energy maintained lower values and dissipated rapidly in time. For Case 3 the flammable mass and available energy reached dangerous levels which persisted over the length of the simulation. It was assumed the Case 1 overpressures would be negligible because the total flammable mass was less than 0.5 kg. The overpressure values are displayed in Figure 42. The overpressure was

calculated assuming that the cloud was ignited after 40 seconds, corresponding to maximum flammable mass. The ignition point was assumed to be at the center of tunnel at the top of the bus.

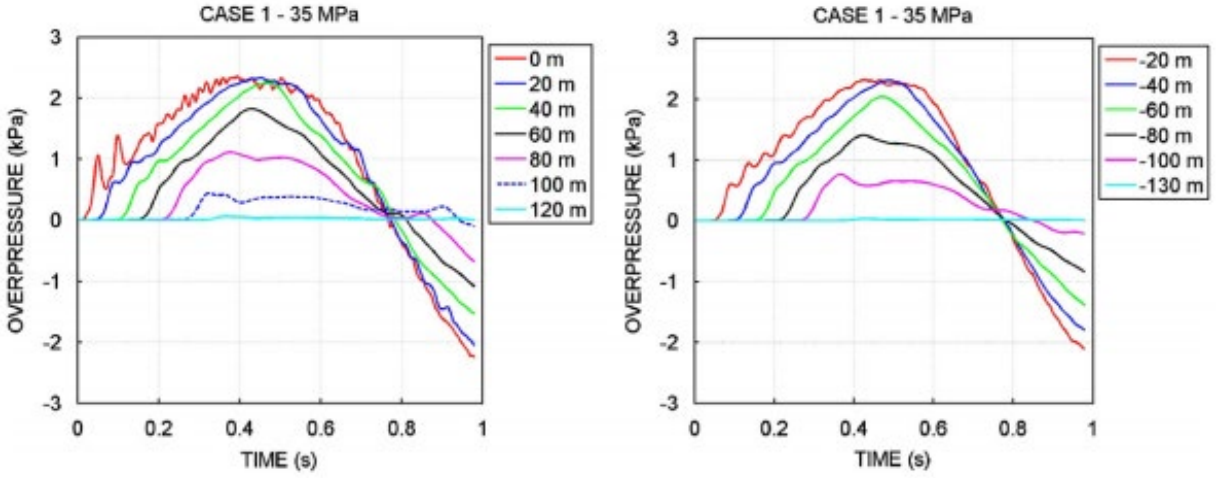

Figure 41: Overpressure values up and down tunnel of the bus for release Case 1 (from [55]

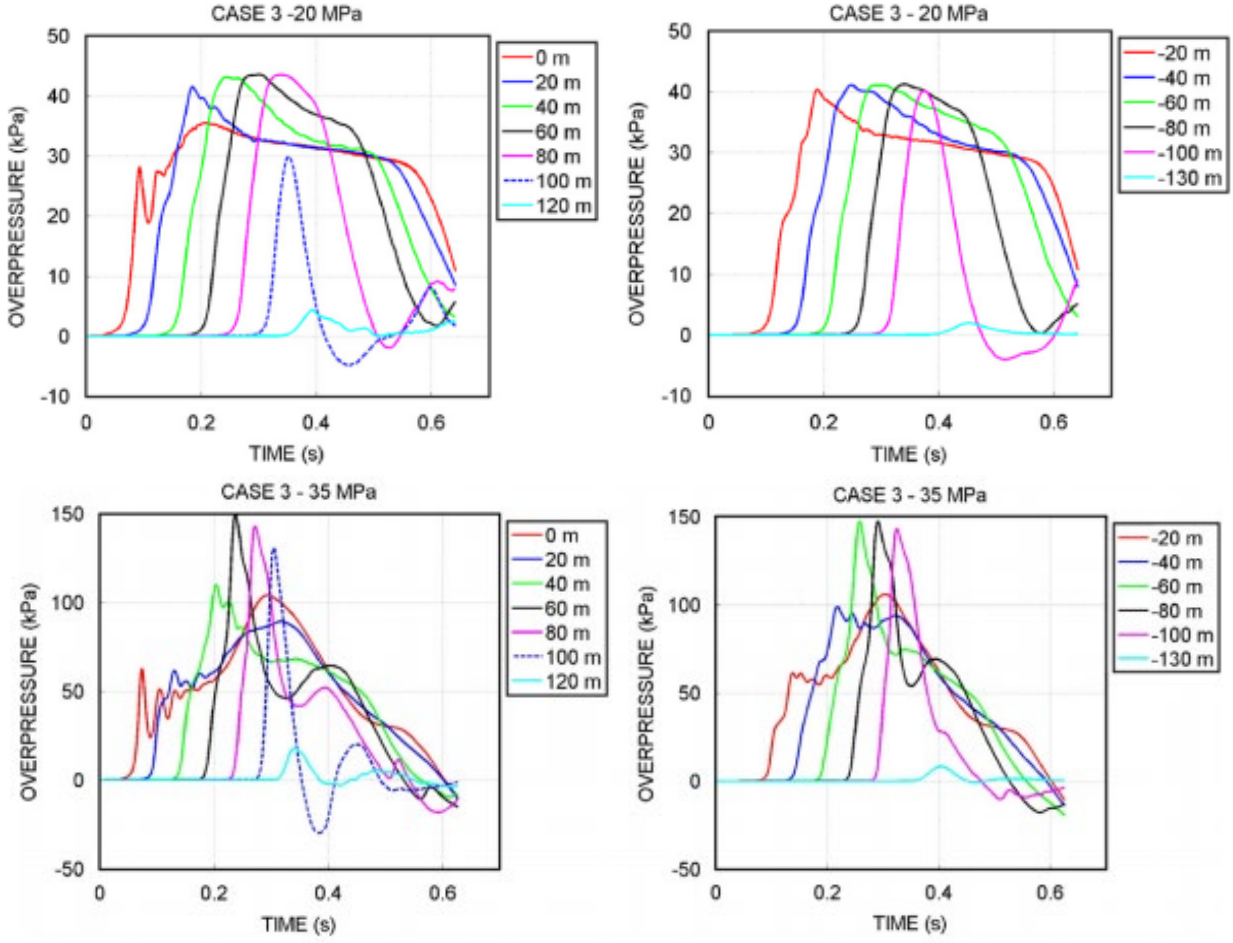

Figure 42: Overpressure values up and down tunnel of the bus for release Case 3 (from [55])

When reviewing these overpressure values, it is important to keep in mind what pressure values correlate to what level of property damage or human hazard. The tables listed in Section 1.2 help understand the damage and tenability thresholds. Case 3 scenario yields overpressure values capable of rupturing eardrums and creating harmful glass splinters up to a distance 80-100 m from the ignition point. Note that the range for the eardrum rupture threshold reported in Table 1 is 16.5-19.3 kPa. For the 35 MPa scenario, the overpressure goes into the threshold for fatality per Table 1. Venetsanos et al. [55] states that the blast wave maintains its strength for long distances inside of tunnels due to the high levels of confinement compared with urban environments where blast waves decay quicker. In addition to overpressure, Venetsanos et al. [55] reported the fireball length along the tunnel, the results for each scenario are displayed in Table 14.

Table 14: Combustion results within tunnel (from [55])

Scenario				Effect	
Case	Fuel	Pressure (MPa)	Energy (MJ)	Fireball Length along the tunnel (m)	Overpressure Peak overpressure (kPa)
1	H_2	20	346	62	2.3
		35	377	58	2.3
		70	448	47	2.3
	NG	20	19	S	S
3	H_2	20	3890	220[a]	42.5
		35	3900	285[a]	150
		70	NM	NM	NM
	NG	20	5380	198	45

Notes: S: Small flammable mass. Calculations were not performed, as the overpressures and fireball size were not expected to be significant. NM: Not modelled. Typical overpressure effects (based on various scientific sources): 2 kPa: Threshold of window breakage. 21 kPa: Threshold of eardrum rupture and moderate building damage. 35 kPa: Severe building damage, i.e. unusable.

[a]The flame extends beyond the limits of the tunnel (tunnel length = 212 m).

For the Case 3 model, the hydrogen combustion produced a flame length which traveled farther than the length of the tunnel, 220 m for the 20 MPa and 285 m for the 35 MPa case of the total 212 m. The flame length for Case 1 hydrogen combustion was reported as 58 m for the 20 MPa and 47 m for the 35 MPa. It is worth noting that in this study, Case 3 represents an implausible scenario of rapid and complete fuel release, ignition when the peak flammable mass is present, and static air within the tunnel. This study further identifies the importance ventilation plays on mitigating risk during an accidental release of fuel in a tunnel.

3.3. Analysis

Multiple analyses have been performed to evaluate the risk associated with hydrogen vehicles in tunnels. One analysis was performed to characterize the most likely consequence of an accident by developing an event sequence diagram and further characterizing severe consequence scenarios. It was shown that the most likely consequence is no additional hazard from the hydrogen (see Section 3.3.1). Another assessment was performed to evaluate the consequence of a delayed ignition of hydrogen released from several different types of vehicles (both cars and buses with compressed hydrogen, as well as a car with LH_2 fuel). It was shown that the maximum pressure loads resulting from ignition from a hydrogen cloud would be insignificant (see Section 3.3.2). Another analysis evaluated the possible incidents and consequences of hazardous events in a tunnel for several different alternative fuel vehicles. This analysis showed that although the HRR is higher for hydrogen when compared to other fuels, the overpressure is relatively low (see Section 3.3.2).

3.3.1. Hydrogen FCEV Tunnel Risk Analysis

A risk analysis was performed to estimate what scenarios were most likely to occur in the event of a hydrogen FCEV accident in a tunnel by Ehrhart et al. [38]. An event sequence diagram for a hydrogen vehicle accident was developed for a hydrogen FCEV accident in a tunnel, including all outcomes along with associated values and probabilities. Figure 43 shows the event sequence diagram developed in the risk analysis.

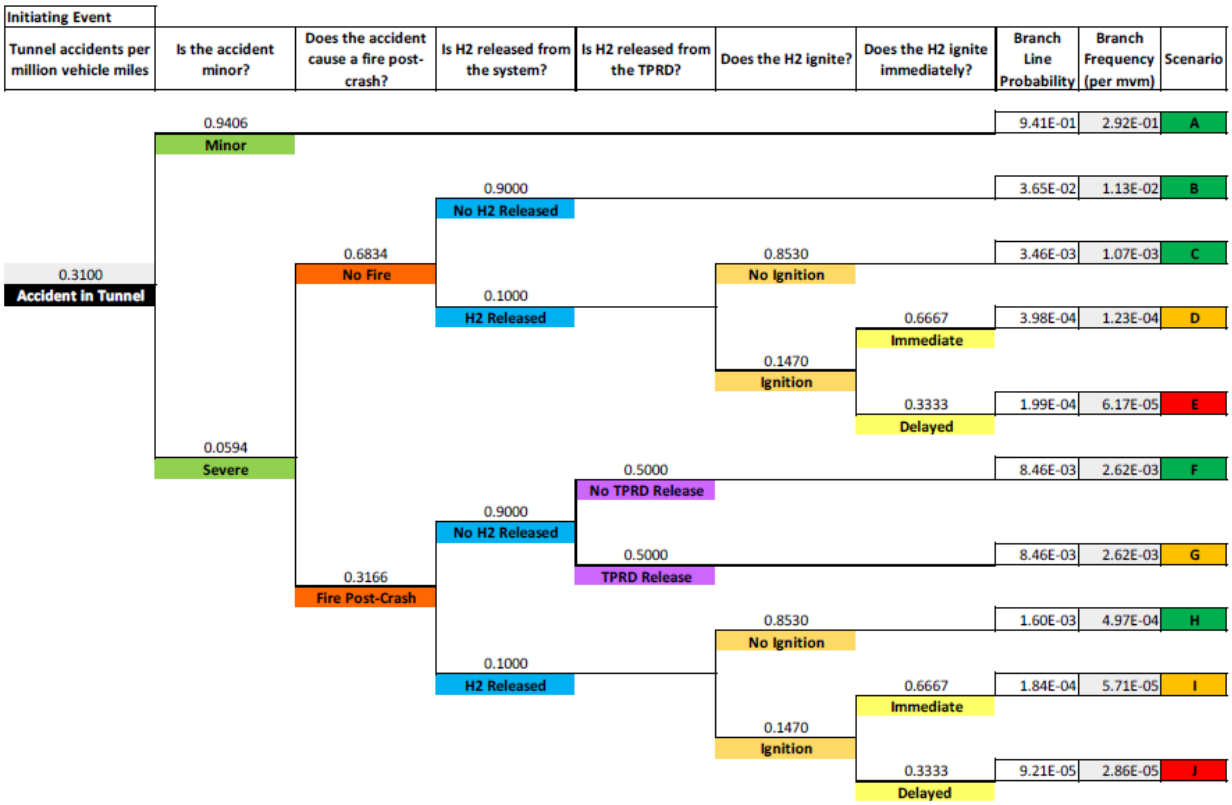

Figure 43: Event Sequence Diagram for a Hydrogen FCEV in a Tunnel (from [38])

Each event was evaluated to determine whether the respective scenario warranted further characterization with heat transfer and CFD models. Based on an evaluation of the risk of each scenario (both the likelihood and consequence), the scenario evaluated further with modeling was a hydrogen vehicle in an accident exposed to a resulting fire. A typical hydrogen FCEV was considered in this analysis, with a 125 L, 70 MPa tank of hydrogen with a typical TPRD orifice of 2.25 mm. Note that due to computational limitations, the smallest reasonable tank orifice diameter that can be modeled is 5.25 cm. This is conservative because the velocity was kept the same for the larger diameter, and so the mass flow and total heat release are larger than what is expected for the realistic 2.25 mm tank orifice diameter. Taking this into account, the worst-case scenario is based on a 5.25 cm release diameter with a constant velocity of 700 m/s. Conservative assumptions were made in terms of the hydrogen fuel released from the TPRD, including having the vehicle flipping over in the crash to orient the jet flame toward the ceiling of the tunnel. Three Boston tunnels with different structural configurations were investigated: the CANA Tunnel, the Ted Williams Tunnel, and the Sumner Tunnel [38]. See Section 0 for information on the CFD, heat transfer, and solid mechanics modeling used for this risk analysis.

The results show that the most likely consequence is no additional hazard from the hydrogen, although some factors need additional data and study to validate. This includes minor crashes and scenarios with no release or ignition. When the hydrogen does ignite, it is most likely a jet flame from the pressure relief device release due to a primary hydrocarbon fire. This scenario was considered in detailed modeling of specific tunnel configurations. Localized concrete spalling may result where the jet flame impinges the ceiling, but this is not expected to occur with ventilation. Structural epoxy remains well below the degradation temperature. The total stress on the steel structure will not be compromised. It is important to note that this study took a conservative approach in several factors, so observed temperatures should be lower than predicted by the models [38].

3.3.2. Hydrogen Vehicle Explosion Risk in Tunnels

An assessment was performed to evaluate the risk of explosion for hydrogen vehicles in tunnels. For all accident scenarios, the hydrogen release is attributed to the activation of the pressure relief device. Two different hydrogen vehicles were evaluated: 1) a city bus with 40 kg H_2 at a storage pressure of 350 bar, and 2) a car with 5 kg H_2 at a storage pressure of 700 bar. Additionally, two different tunnel layouts (horseshoe and rectangular) and several longitudinal ventilation conditions were considered. The following hydrogen release scenarios were evaluated [49]:

1. Hydrogen Passenger Vehicle (vent up) releasing 5 kg of H_2 for 84s
2. Hydrogen Passenger Vehicle(vent down) releasing 5 kg of H_2 for 84s
3. Hydrogen Bus releasing 5 kg of H_2 for 147s
4. Hydrogen Bus releasing 20 kg of H_2 for 147s
5. Hydrogen Passenger Vehicle releasing 10 kg of LH2 for 900s

The ignition probabilities and intensities were developed from information relevant to the oil and gas industry. Initially, stoichiometric gas clouds of different sizes are considered to explode to calculate the maximum overpressure near the tunnel ceiling [49]. As a refinement, dispersion modeling was performed to determine the gas cloud size and hydrogen concentration that can be realistically expected. CFD modeling was used to evaluate both the dispersion and explosion simulations for each of the scenarios described previously (see Section 3.2.2).

The worst-case deterministic evaluation of each of the scenarios involved the tunnel filling with stochiometric hydrogen gas clouds of varying size. This showed unacceptable results in terms of very high overpressures. However, a dispersion study was performed to determine a more realistic gas cloud from hydrogen release and their subsequent ignition. This more realistic evaluation showed that the worst-case overpressures were reduced by two orders of magnitude. Moreover, a probabilistic study was performed that reduced the expected risk of an explosion due to a hydrogen vehicle even more. The maximum pressure loads (between 0.1 barg [threshold for skin laceration from flying glass] and 0.3 barg [serious wounds from flying glass near 50% probability]) predicted by the simulations could be significant [49].

3.3.3. Fire and Explosion Hazards in Tunnels of Alternative Fuel Vehicles

An analysis of the possible incidents and consequences of hazardous events in a tunnel was evaluated for several different alternative fuel vehicles, including gaseous and liquid hydrogen

vehicles by Li [56]. The likelihood of the events was not evaluated, but event trees were defined for both liquefied fuel vehicles and compressed gas vehicles (see Figure 44 and Figure 45).

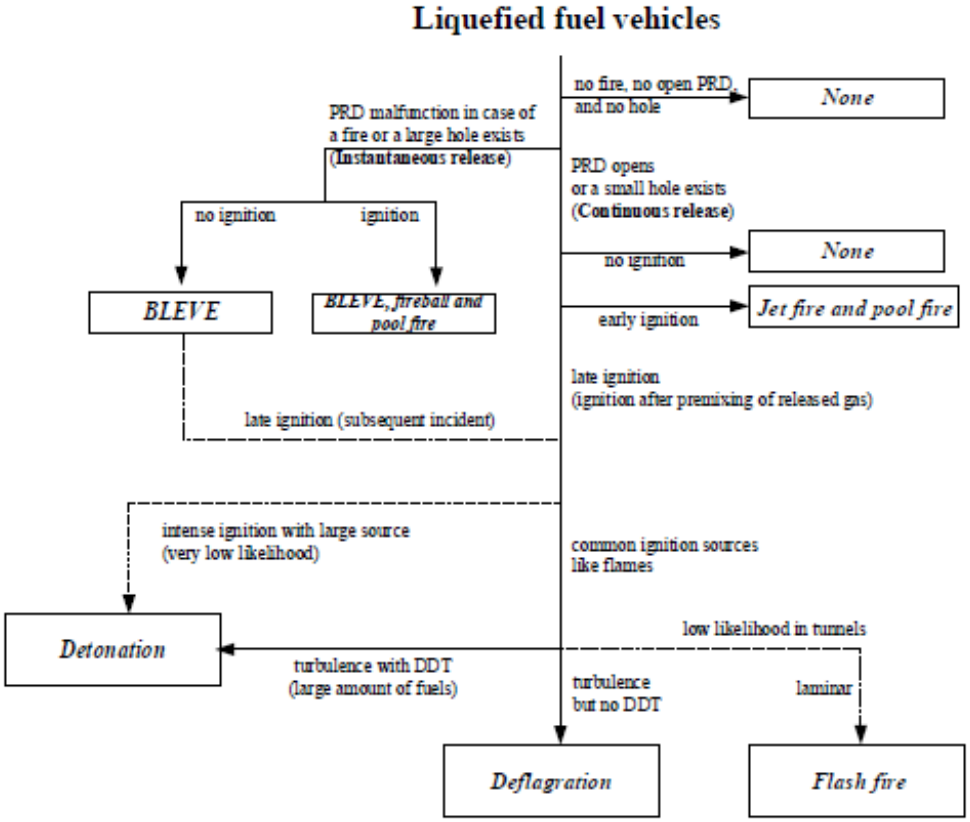

Figure 44: Liquefied Fuel Vehicle Event Tree for Incidents in Tunnels (from [56])

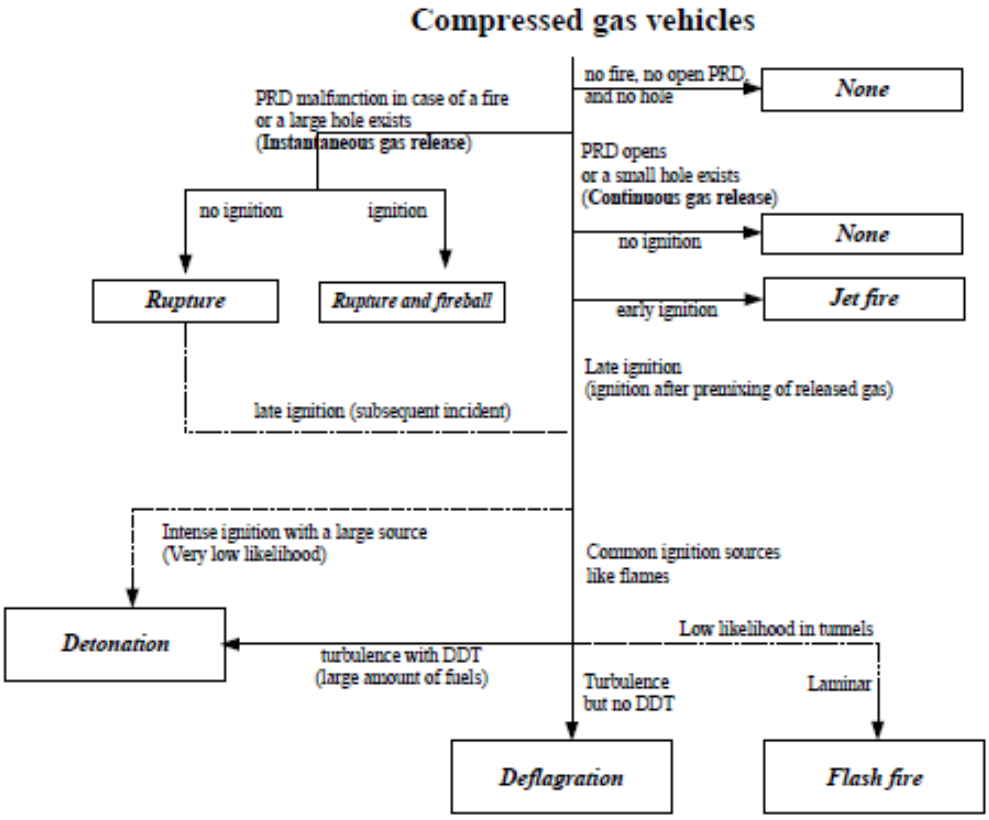

Figure 45: Compressed Gas Vehicle Event Tree for Incidents in Tunnels (from [56])

Each event was evaluated through simple modeling to determine the potential consequence. An analysis of spilled fuel fires for liquid hydrogen vehicles showed that the heat release rate per unit fuel area of liquid hydrogen is around 60 times higher than ethanol and methanol. For jet fires, the analysis showed that the heat release rates for hydrogen vehicles were significantly higher than those of compressed natural gas tanks, while the flame length was only slightly greater. Figure 47 shows the peak overpressure as a function of distance resulting from rupture of the pressure vessel. As shown, the overpressure decreases rapidly within the first 50 m [56].

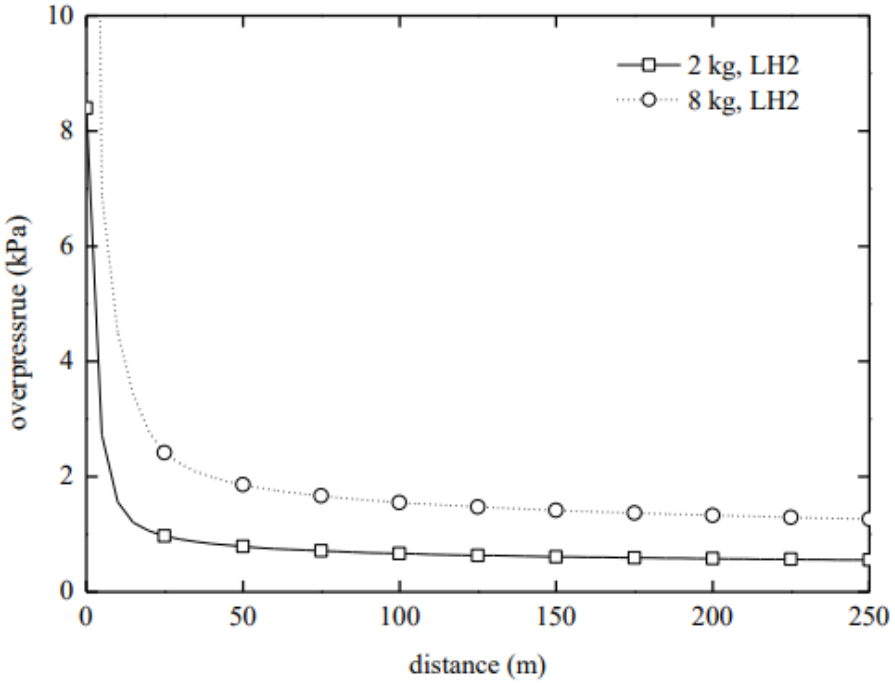

Figure 46: Overpressure vs. Distance for Liquid H_2 tank at 350 bar (from [49])

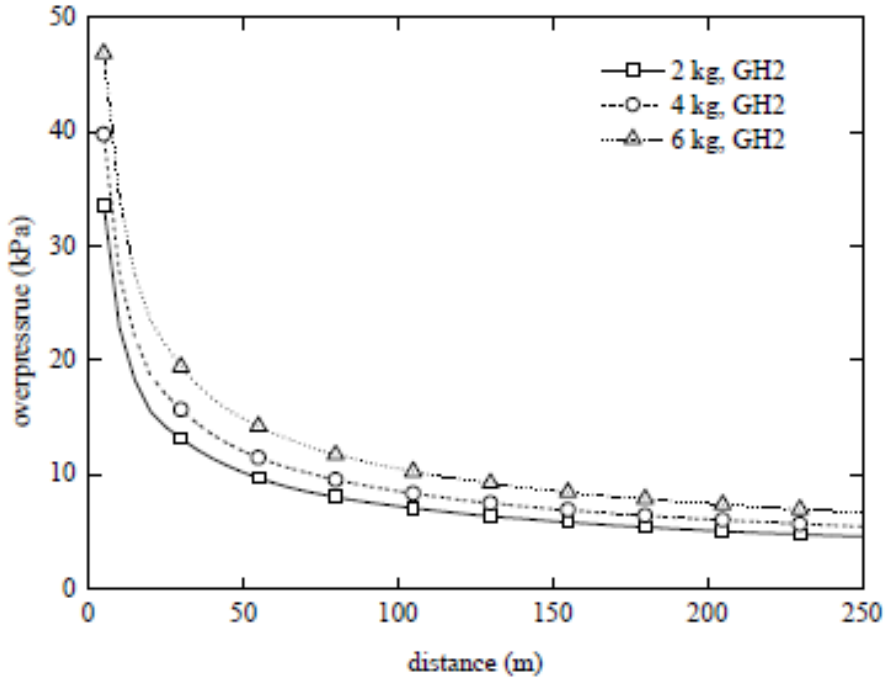

Figure 47: Overpressure vs. Distance for Gaseous H_2 tank at 350 bar (from [49])

Finally, the peak overpressure resulting from a gas cloud explosion was evaluated for both gaseous and liquefied hydrogen. The overpressures for each case were relatively low when compared to the other alternative fuels such as natural gas due to the small fuel mass for the hydrogen case which leads to lower explosion energy [56].

4. CONCLUSION

Through this literature study, it was found that there are several existing studies that evaluate the failure modes and consequences associated with hydrogen fuel cell electric vehicles (FCEVs) in tunnels. There have been multiple experimental studies that have investigated overpressures resulting from delayed hydrogen ignition, HRR, hydrogen dispersion, and thermal effects of jet fires. Modeling studies have been conducted on the consequences of release, including hydrogen accumulation followed by ignition and the resulting overpressure. Also, risk analysis has been conducted on the thermal effects on tunnel components from a jet fire rather and identification of release events that could occur. Additionally, analysis has been performed to quantify probabilities and likelihoods for these various events.

Conclusions about important variables can be derived from comparison of the different literature. As ventilation increases, the overpressure decreases in a congested area [43] [44]. However, CFD results of a tunnel including vehicles as blockage show that the overpressure stays about the same. This could mean that ventilation is a stronger factor in varying the overpressure. The exceedance curve shown in Figure 21 shows the various hydrogen leak scenarios and the frequency of each one. In the event of a leak, the layer height and concentration were used to create a matrix to understand how different leak scenarios might lead to various deflagrations or even detonations [45].

4.1. Research Gaps

Although significant work has been accomplished, there are still areas that should be evaluated further. The following criteria were evaluated to determine where research gaps may exist regarding hydrogen FCEVs in tunnels.

a) Scenario Identification

b) Failure Modes

c) Consequences

d) Validation

In terms of scenario identification included in this literature survey, the scenarios that lead to a failure mode have been identified as impacts to the vehicle or failure of the TPRD, hardware degradation or failure, and operator error which may lead to a release of fuel. Fault trees for both liquid and gaseous fuel release can be seen in Figure 44 and Figure 45. Failure modes were addressed through several studies evaluating the mechanism and consequences associated with hydrogen FCEVs in tunnels. The failure modes with potentially hazardous consequences identified in the scenario identification effort included a release with either immediate or delayed ignition.

The measurements of the consequences of the failure mode include overpressure, HRR, hydrogen dispersion, and resulting structural damage determine the extent of the hazard. There are several variables that effect the magnitude of the consequence: hydrogen quantity released, ventilation, obstructions, ignition time, tunnel geometry, etc. Results of the consequences include overpressures that range from 34 kPa [49] to over 100 kPa [55], HRR that can peak near 16 MW [46], and fireballs that can exceed 250 m long [55].

Also, validation of the results has been achieved through comparison studies between the modeling and experiments with regard to various consequences like HRR [46].

The research of hydrogen FCEVs in tunnels has evaluated, in some manner, a significant combination of failure modes, consequences, and influencing variables. Despite this, the following research gaps were identified:

- Temperature and thermal effects to structures. A diagnostic to the consequence of a failure mode is temperature or thermal effects. Although this has been addressed in a single modeling/analysis report, additional research should be conducted on this topic.
- Ventilation effects. The study of spontaneous ignition was conducted at ambient conditions outdoors. The effect that ventilation in a tunnel has on the results could be evaluated.
- Hydrogen-specific fires. The power associated with the fires in Section 3.2.6 should be related to specific hydrogen vehicle types (e.g., cars, buses, etc.).
- The effect of deflagration/detonation on structural components of a tunnel for each of the different hydrogen vehicle classes.
- The effect of overpressure effects on life safety to people within the tunnel.
- The extent to which hydrogen can accumulate due to partial confinement and restriction, rather than complete confinement.
- Additional attention should be given to the size or class of the vehicle. As vehicular class increases so does the amount of stored fuel. Several different classes of vehicles were evaluated in the studies, including hydrogen cars and buses, liquid hydrogen cars, and multiple hydrogen cars on a cargo truck.

4.2. Future Work

The International Conference on Hydrogen Safety (ICHS) in 2019 showcased a variety of topics for hydrogen safety [57]. As the papers are published from this event, some of the identified research gaps may be addressed. Some of these gaps as well as others will be addressed in the output of the current HyTunnel-CS project [58]. The intent of this project is to perform research regarding hydrogen powered vehicle safety in tunnels and confined spaces. The goal is for hydrogen vehicles entering underground environments to maintain comparable risk as fossil fuels. Experiments in tunnels, modeling using tools such as CFD programs, and analysis using risk assessment methodologies will be covered in this project.

The HyTunnel-CS project has identified the following work packages (WP) to address research gaps:

WP1 – The state-of-the-art in safety provisions for underground transportation systems and accident scenarios prioritization

WP1 will review the state-of-the-art in safety provisions for underground transportation systems and the accident scenarios prioritization will aid at identifying the knowledge gaps in both safety science and regulations, codes, and standards to be addressed

WP2 – Effect of mitigation systems on hydrogen release and dispersion in confined spaces

An intensive experimental program empowered by theoretical and numerical studies will be performed under this work package. The work addresses the knowledge gaps highlighted in WP1 and the development of novel engineering solutions for the prevention and mitigation of accident involving hydrogen releases.

WP3 – Thermal and pressure effects of hydrogen jet fires and structure integrity

Under this work package jet fires will be investigated through a comprehensive set of experimental, theoretical, and numerical studies to improve the principal understanding of hydrogen jet fire on life safety provisions in underground transportation systems and their structural integrity.

WP4 – Explosion prevention and mitigation

WP4 investigates explosion prevention and mitigation through numerous experimental tests realized in tunnels and other confined spaces and theoretical and numerical studies on accident scenarios involving hydrogen tanks. The aim of the WP is to provide engineering tools to evaluate the associated hazards, as well as innovative preventive and mitigation solutions and to improve the principal understanding of hydrogen explosion hazards in tunnels and similar confined spaces using complementarities of theoretical, numerical and experimental studies.

WP5 – First responders' intervention strategies and tactics for hydrogen accidents in underground transportation systems and risk assessment

Under WP5, the research findings from WPs 2-4 will be translated into suitable information, guidelines, and recommendations for first responders intervening in an accident involving hydrogen-powered vehicles in tunnels or other confined spaces. This includes examining and supplementing available knowledge in such a way that it can be taught to all first responders and can also be practically applied by them.

WP6 through WP8 –Outreach/Dissemination, Management, and Ethics are not summarized since these are not technical research gaps.

5. REFERENCES

[1] "International Partnership for Hydrogen and Fuel Cells in the Economy," 2020. [Online]. Available: https://www.iphe.net/ . [Accessed 02 04 2020].

[2] A. K. Coker, "9 - PROCESS SAFETY AND PRESSURE-RELIEVING DEVICES," in *Ludwig's Applied Process Design for Chemical and Petrochemical Plants (Fourth Edition)*, Burlington, Gulf Professional Publishing, 2007, pp. 575-770.

[3] California Institute of Technology, "Flammability and Explosion Limits," [Online]. Available: https://shepherd.caltech.edu/EDL/PublicResources/flammability.html. [Accessed 05 12 2019].

[4] W. D. Manha, "Chapter 20 - Propellant Systems Safety," in *Safety Design for Space Systems*, Oxford, Butterworth-Heinemann , 2009, pp. 661-694.

[5] M. Huth and A. Heilos, "14 - Fuel flexibility in gas turbine systems: impact on burner design and performance," in *Modern Gas Turbine Systems*, Cambridge, Woodhead Publishing Limited, 2013, pp. 635-684.

[6] G. Jomaas, "Fundamentals of Premixed Flames," in *SFPE Handbook 5th Edition*, New York City, Springer, 2016, pp. 373-395.

[7] NOAA Office of Response and Restoration, "Overpressure Levels of Concern," NOAA Office of Response and Restoration, [Online]. Available: https://response.restoration.noaa.gov/oil-and-chemical-spills/chemical-spills/resources/overpressure-levels-concern.html. [Accessed 20 09 2019].

[8] MIT Thermodynamics and Propulsion, "Thermodynamics and Propulsion," MIT Thermodynamics and Propulsion, [Online]. Available: https://web.mit.edu/16.unified/www/FALL/thermodynamics/notes/node111.html. [Accessed 20 09 2019].

[9] DOE Office of Energy Efficiency and Renewable Energy's Fuel Cell Technologies Office, "H2 Tools," DOE Office of Energy Efficiency and Renewable Energy's Fuel Cell Technologies Office, [Online]. Available: https://h2tools.org/hyarc/calculator-tools/lower-and-higher-heating-values-fuels. [Accessed 20 09 2019].

[10] National Institute of Standards and Technology, "Fire Dyanmics," NIST, 17 07 2018. [Online]. Available: https://www.nist.gov/el/fire-research-division-73300/firegov-fire-service/fire-dynamics. [Accessed 01 10 2019].

[11] National Fire Protection Association, NFPA 921: Guide for Fire and Explosion Investigations, Quincy, 2017.

[12] EUROPEAN INDUSTRIAL GASES ASSOCIATION AISBL , "DETERMINATION OF SAFETY DISTANCES IGC Doc 75/07/E," Brussels, 2007.

[13] DOE Energy Efficiency & Renewable Energy, "Maps and Data - Vehicle Weight Classes & Categories," DOE Energy Efficiency & Renewable Energy, [Online]. Available: https://afdc.energy.gov/data/10380. [Accessed 19 09 2019].

[14] DOE Energy Efficiency & Renewable Energy, "Alternative Fuels Data Center," [Online]. Available: https://afdc.energy.gov/data/. [Accessed 25 09 2019].

[15] National Renewable Energy Laboratory, On-Road Fuel Cell Electric Vehicles Evaluation: Overview, March 2019.

[16] Hyundai Motor America, "Hyundai ix35 Fuel Cell," Hyundai Media Center, [Online]. Available: https://www.hyundainews.com/en-us/releases/1624. [Accessed 04 04 2020].

[17] J. Kurtz, S. Sprik, G. Saur and S. Onorato, "On-Road Fuel Cell Electric Vehicles Evaluation: Overview NREL/TP-5400-73009," National Renewable Energy Laboratory, March 2019.

[18] California Air Resources Board, 2018 Annual Evaluation of Fuel Cell Electric Vehicle Deployment & Hydrogen Fuel Station Network Development, July 2018.

[19] Plug Power, "WHO'S USING GENDRIVE?," [Online]. Available: https://www.plugpower.com/customer/whos-using-gendrive/. [Accessed 03 02 2020].

[20] Fuel Cell & Hydrogen Energy Association, "[Company] Celebrates National Hydrogen and Fuel Cell Da," [Online]. Available: http://www.fchea.org/sample-press-release-2019. [Accessed 03 02 2020].

[21] International Partnership for Hydrogen and Fuel Cells in the Economy, [Online]. Available: https://www.iphe.net/united-states. [Accessed 20 April 2020].

[22] N. LePan, "The Evolution of Hydrogen: From the Big Bang to Fuel Cells," Visual Capitalist, 23 4 2019. [Online]. Available: https://www.visualcapitalist.com/evolution-of-hydrogen-fuel-cells/. [Accessed 3 1 2020].

[23] I. Abe, Energy Carriers and Conversion Systems - Vol. I - Physical and Chemical Properties of Hydrogen.

[24] College of the Desert, Hydrogen Fuel Cell Engines and Related Technologies, Module 1: Hydrgoen Properties, December 2001.

[25] Matheson Tri Gas, "Lower and Upper Explosive Limits for Flammable Gases and Vapors (LEL/UEL)," Matheson Tri Gas, [Online]. Available: https://www.mathesongas.com/pdfs/products/Lower-(LEL)-&-Upper-(UEL)-Explosive-Limits-.pdf. [Accessed 04 12 2019].

[26] R. Ono, N. Masaharu, S. Fujiwara, S. Horiguchi and T. Oda, "Minimum ignition energy of hydrogen–air mixture: Effects of humidity and spark duration," *Journal of Electrostatics,* vol. 65, no. 2, pp. 87-93, 2007.

[27] C. J. Coronado, J. A. Carvalho Jr., J. C. Andrade, E. V. Cortez, F. S. Carvalho, J. C. Santos and A. Z. Mendiburu, "Flammability limits: A review with emphasis on ethanol for aeronautical applications and description of the experimental procedure," *Journal of Hazardous Materials,* vol. 32, no. 54, pp. 241-242, 2012.

[28] R. Eckhoff, M. Ngo and W. Olsen, "On the minimum ignition energy (MIE) for propane/air," *Journal of Hazardous Materials,* vol. 175, no. 1-3, pp. 293-297, 2010.

[29] Air Products and Chemicals Inc., *Ignition Energy of H2, CH4, and gasoline with Air,* Air Products, 2001.

[30] The Engineering ToolBox, "Adiabatic Flame Temperatures," [Online]. Available: https://www.engineeringtoolbox.com/adiabatic-flame-temperature-d_996.html. [Accessed 04 12 2019].

[31] H. Haase, Electrostatic Hazards: their evaluation and control, Verlag Chemie, 1977.

[32] V. Babrauskas, Ignition Handbook, 2003.

[33] The Engineering ToolBox, "Fuels and Chemicals - Autoignition Temperatures," [Online]. Available: https://www.engineeringtoolbox.com/fuels-ignition-temperatures-d_171.html. [Accessed 04 12 2019].

[34] NFPA, NFPA 77: Recommended Practice on Static Electricity, Quincy, 2019 Ed..

[35] C. LaFleur, "Large Scale Hydrogen System Safety Issues," *Chemical Engineering Progress,* vol. 115, no. 8, pp. 42-46, 2019.

[36] National Fire Protection Association, NFPA 2: Hydrogen Technologies Code, Quincy, 2020 Edition.

[37] Global Registry, "Addendum 13: Global technical regulation No. 13 Global technical regulation on hydrogen and fuel cell vehicles," UNITED NATIONS, 2013.

[38] Sandia National Laboratories, Hydrogen Fuel Cell Electric Vehicle Tunnel Safety Study, October 2017.

[39] F. Dryer, M. Chaos, Z. Zhao, J. Stein, J. Alpert and C. Homer, "Spontaneous Ignition of Pressurized Releases of Hydrogen and Natural Gas into Air," *Combust. Sci. and Tech. 2007,* 2007.

[40] M. Groethe, E. Merilo, J. Colton, S. Chiba, Y. Sato and H. Iwabuchi, "Large-scale Hydrogen Deflagrations and Detonations," *Int J Hydrogen Energy,* vol. 32, no. 13, pp. 2153-2133, 2007.

[41] J. M. Chock, "Review of Methods for Calculating Pressure Profiles of Explosive Air Blast and its Sample Application," Virginia Polytechnic Institute and State University, Blacksburg, 1999.

[42] F. Tamanini, "Scaling parameters for vented gas and dust explosions," *Journal of Loss Prevention in the Process Industries,* vol. 14, pp. 455-461, 2001.

[43] G. Houf, G. Evans, E. Merilo, M. Groethe and S. James, "Releases from Hydrogen Fuel-cell Vehicles in Tunnels," *Int J Hydrogen Energy,* vol. 37, pp. 715-719, 2012.

[44] S. Kumar, S. Miles, P. Adams, A. Kotchourko, D. Heldey, P. Middha, V. Molkov, A. Teodorczyk and M. Zenner, "HyTunnel Project to Investigate the use of Hydrogen Vehicles in Road Tunnels," in *3rd International Conference on Hydrogen Safety (ICHS3)*, 2009.

[45] A. Friedrich, J. Grune, T. Jordan, A. Kotchourko, N. K. M. Kotchourko, K. Sempert and G. Stern, "EXPERIMENTAL STUDY OF HYDROGEN-AIR DEFLAGRATIONS IN FLAT LAYER," in *Proc. 2nd ICHS International conference on hydrogen safety*, San Sebastian, 2007.

[46] M. Seike, Y. Ejiri, N. Kawabata, M. Hasegawa and H. Tanaka, "Fire experiments of carrier loaded FCV in full-scale model tunnel - Estimation of heat release rate and smoke generation rate," in *Third International Converence on Fire in Vehicles*, Berlin, Germany, 2014.

[47] M. Royle, L. Shirvill and T. Roberts, "Vapour cloud explosions from the ignition of methane/hydrogen/air mixtures in a congested region," in *International Conference on Hydrogen Safety*, 2007.

[48] B. D. Ehrhart, D. M. Brooks, A. B. Muna and C. B. LaFleur, "Risk Assessment of Hydrogen Fuel Cell Electric Vehicles in Tunnels," *Fire Technology,* pp. 1-22, 2019.

[49] P. Middha and O. Hansen, "CFD Simulation Study to Investigate the Risk from Hydrogen Vehicles in Tunnels," *Int J Hydrogen Energy,* vol. 34, pp. 5875-5876, 2009.

[50] I. Tolias, A. Venetsanos, N. Markatos and C. Kiranoudis, "CFD Modeling of Hydrogen Deflagration in a Tunnel," *Int J Hydrogen Energy,* vol. 39, pp. 20538-20546, March 2014.

[51] G. Houf, G. Evans, E. Merilo, M. Groethe and S. James, "Releases from Hydrogen Fuel-cell Vehicles in Tunnels," *Int J Hydrogen Energy,* vol. 37, pp. 715-719, 2012.

[52] H. Bie and Z. Hao, "Simulation Analysis on the Risk of Hydrogen Releases and Combustion in Subsea Tunnels," *Int J Hydrogen Energy,* 2016.

[53] Y. Wu, "Assessment of the impact of ject flame hazard from hydrogen cars in road tunnels," *Transportation Research Part C,* vol. 16, pp. 246-254, 2008.

[54] S. Mukai, J. M. H. Suzuki, K. Oyakawa and S. Watanabe, "CFD simulation on diffusion of leaked hydrogen caused by vehicle accident in tunnels," 2005.

[55] A. Venetsanos, D. Baraldi, P. Adams, P. Heggem and H. Wilkening, "CFD modelling of hydrogen release, dispersion and combustion for automotive scenarios," *Journal of Loss Preventation in the Process Industries,* vol. 21, no. 2, pp. 162-184, 2008.

[56] Y. Z. Li, "Fire and Explosion Hazards of Alternative Fuel Vehicles in Tunnels".

[57] ICHS, [Online]. Available: https://hysafe.info/ichs2019/. [Accessed 24 03 2020].

[58] HyTunnel-CS, "About HyTunnel-CS," HyTunnel-CS, 2019. [Online]. Available: https://hytunnel.net/?page_id=31. [Accessed 26 09 2019].